Theory of action potentials

Romain Brette

July 19, 2016

Contents

Chapter 3

Action potential of an isopotential membrane

3.1 Experimental preparations

3.1.1 The space-clamped squid giant axon

The first quantitative model of action potentials was a model of the action potential of the space-clamped squid giant axon, conceived and experimentally tested by Hodgkin and Huxley (Hodgkin and Huxley, 1952a). By *space-clamped*, we mean that the intracellular potential of the axon is maintained spatially uniform over its length. The Hodgkin-Huxley model was the culmination of a series of 5 papers (120 pages) by Hodgkin, Huxley and Katz, published in the Journal of Physiology in 1952 (Hodgkin et al., 1952; Hodgkin and Huxley, 1952c,b,d,a).

As already discussed in chapter **??**, the squid giant axon had been introduced in the 1930s as a model of choice for electrophysiology because of its very large diameter (up to 1 mm). It is a rather peculiar axon as it is one of the few exceptions to the neuron doctrine, i.e., it is not a neurite of a cell, but it results from the fusion of hundreds of cells, a syncytium (Young, 1936) (see Fig. **??**). In addition, the Hodgkin-Huxley model, which we will present in

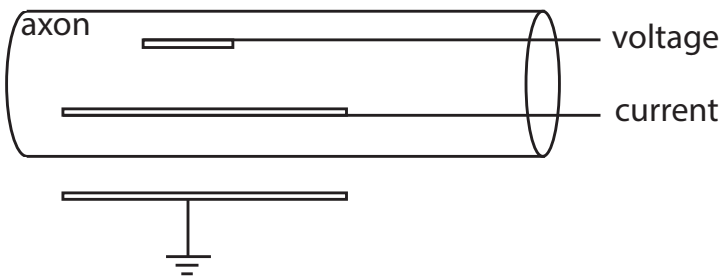

Figure 3.1: Electrophysiological apparatus used by Hodgkin and Huxley to measure current-voltage relationships in the squid giant axon (Hodgkin et al., 1952). The current wire is exposed over 15 mm.

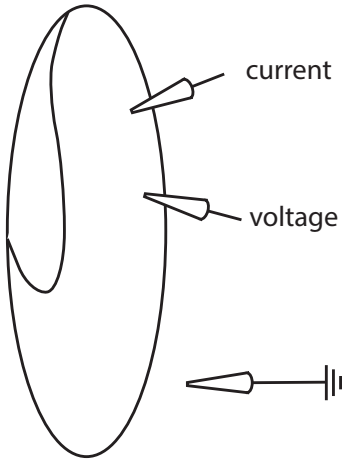

Figure 3.2: Experimental configuration for electrophysiology in Paramecium.

detail in section 3.4, was established from the space-clamped axon, an experimental preparation where the axon's intracellular medium is made isopotential by inserting a metal wire inside it. Figure 3.1 is a simplified representation of the experimental apparatus: two wires are inserted into the axon, one in which current is passed and another one used to measure intracellular potential. Reference electrodes are placed outside the axon. The current wire is exposed over 15 mm, and this makes the intracellular medium of the axon isopotential. This configuration was critical to measure current-voltage relationships of the membrane: without the space clamp, currents would be measured coming from different portions of the membrane where the membrane potential is uncontrolled. What textbooks usually refer to as the Hodgkin-Huxley model is thus not exactly a neuron model (the squid giant axon does not belong to a neuron anyway), but a model of the space-clamped squid giant axon. Nonetheless, Hodgkin and Huxley also successfully extended their model into a model of the propagating AP of the squid axon (chapter **??**), and the biophysical basis of APs has been shown to be very similar in neurons and all other excitable cells.

3.1.2 Paramecium

In this chapter, we will focus mainly on the squid giant axon. But in parallel, we will also present the action potential of Paramecium for two reasons. First, Paramecium is an isopotential cell in its natural state. Second, the biophysical basis of its action potential is also based on the opening of ionic channels, but the depolarizing phase of the AP is due to the entry of Ca^{2+} ions rather than Na^{+} ions in the squid giant axon. This will illustrate the diversity of action potentials. As mentioned in chapter **??**, calcium APs are also seen in a variety of excitable cells, such as developing neurons, invertebrate muscles and sperm. Calcium channels with similar properties as those of Paramecium are also found in vertebrate neurons.

In the 1960s and 70s, there was a community of electrophysiologists interested in Paramecium for several reasons. One is that there is a direct relation between electrical activity and behavior: the action potential triggers a change in swimming direction (see section **??**). Another one is that electrophysiological recordings are relatively easy to perform because the cell is large: around 200 μm long (remember that the cell body of a neuron is around 30 μm large). Two glass

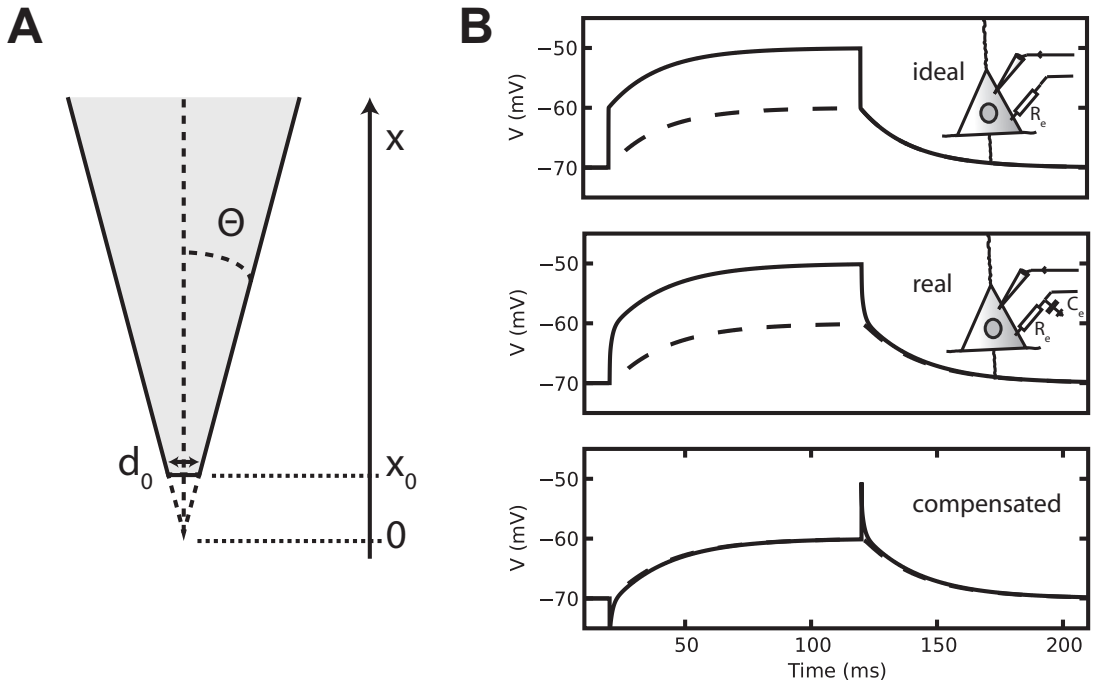

Figure 3.3: Pipette resistance. A, Truncated cone representing the pipette tip. B, Voltage response of a neuron to a current pulse, as measured at the amplifier end (simulated traces), with intracellular potential shown in dashed. Top: the electrode is seen as an ideal resistance; middle: the electrode also has a capacitance; bottom: electrode voltage corrected by the amplifier (*bridge balance* or *series compensation*).

microelectrodes, with very sharp tips that can pierce the membrane, are inserted into the cell (Fig. 3.2). One is used for passing current, the other for recording voltage (the third electrode outside the cell is the reference). By inserting a second voltage electrode on the other side of the cell, it can be checked that the membrane potential is the same at different locations inside the cell[1] (Eckert and Naitoh, 1970). However, Paramecium is not a spatially homogeneous cell since ionic channels responsible for APs in Paramecium are located in the cilia (Ogura and Takahashi, 1976). It might be that cilia are not isopotential.

3.1.3 Electrophysiological techniques

We now present a brief overview of the techniques used to measure electrophysiological properties of membranes. More detail can be found in (Molleman, 2002) for the practical aspects, and in (Brette and Destexhe, 2012) for the technical and modeling aspects.

Pipette resistance

Figure 3.2 shows a typical configuration where current can be injected through an electrode, and the voltage response of the cell is measured at another electrode. We often use the term "electrode" to refer to the pipette, which is a glass capillary that is pulled so as to make a fine tip, while the electrode is more precisely the interface between the wire inside the pipette and the electrolyte. Why do we need two separate electrodes and not just one, in addition to the reference electrode? This is because the electrolyte inside the pipette has an electrical resistance, which depends on the geometry of its tip. It is a good exercise to calculate this resistance, and we will encounter this type of question again when we study cable theory in chapter **??**.

Let us assume that the pipette tip is a truncated cone of tip diameter d_0 and angle θ, defined from the symmetry axis (Figure 3.3A). We cut this cone in thin cylindrical slices of diameter $d(x)$ and thickness dx, where x is distance from the untruncated cone tip. The pipette tip is at distance x_0. What is the resistance of a cylinder? The amount of current that passes through it is proportional to its section area $\pi d^2/4$, and therefore its resistance (inverse of conductance) is inversely proportional to it. Its resistance should be proportional to its length, because resistances in series add. Therefore, the resistance of a thin cylinder should be:

$$R(x) = \frac{4dx}{\pi d(x)^2} R_i$$

where R_i is a proportionality coefficient that we call *intrinsic resistivity*, in Ω.m. This is the resistivity of the electrolyte, with order of magnitude 1 Ω.m. The intracellular and extracellular media also have a resistivity, of roughly the same order, often expressed in Ω.cm (1 Ω.m = 100 Ω.cm). Thus the total resistance of the truncated cone over a length L is:

$$R_e = \frac{4R_i}{\pi} \int_{x_0}^{L} \frac{dx}{d(x)^2}$$

(R_e for electrode resistance).

From $d(x) = x \tan\theta$, we obtain:

$$\begin{aligned} R_e &= \frac{4R_i}{\pi \tan^2\theta} \int_{x_0}^{L} \frac{dx}{x^2} \\ &= \frac{4R_i}{\pi \tan^2\theta} \Big[-\frac{1}{x} \Big]_{x_0}^{L} \\ &= \frac{4R_i}{\pi \tan^2\theta} \Big(\frac{1}{x_0} - \frac{1}{L} \Big) \end{aligned}$$

We can see that if the cone is long enough compared to the tip diameter (which does not exceed a couple of μm), then we can neglect its length. In other words, it does not matter exactly where the wire ends in the pipette. Finally, we use $d_0 = x_0 \tan\theta$ and we get:

$$R_e = \frac{4R_i}{\pi d_0 \tan\theta}$$

The conclusion is that pipette resistance is inversely proportional to tip diameter. For example, with tip diameter 1 μm, $R_i = 1$ Ω.m and $\theta = \pi/4$ (i.e., the pipette makes a right angle), we

[1] More precisely, the variations of membrane potential are identical; the precise value of the membrane potential is not very reliable with sharp microelectrodes because of tip potentials (Brette and Destexhe, 2012).

obtain $R_e \approx 1.3$ MΩ. Microelectrodes used in paramecium, as well as in neurons until the development of the patch-clamp technique (see next section), have a very sharp tip of $0.01 - 0.1$ μm in diameter. They had been developed by Ling and Gerard (1949) by pulling glass capillary tubes, resulting into a very fine tip that can penetrate cell membranes. This produces pipette resistances (also called *electrode resistance* or *series resistance*) of order $10-100$ MΩ. Thus when a current $I = 1$ nA is passed through an electrode with pipette resistance $R_e = 100$ MΩ, there is a potential difference between the electrode (the wire) and the pipette tip of $R_e I = 100$ mV. Thus the electrode potential can be very different from the intracellular potential. An example is shown on Figure 3.3B (top), where a current pulse is injected through the electrode and voltage is measured at the amplifier end: a bias is observed during current injection (real intracellular potential in dashed). There are additional difficulties: the pipette and the amplifier input also have capacitive properties (Fig. 3.3B, middle), there can be voltage offsets due to junction and tip potentials[2] when the cell is impaled, and the resistance generally changes when the electrode penetrates the membrane. The resistance when the intracellular medium is accessed is often called *access resistance*. Thus it is generally preferable to use two electrodes to pass currents and measure voltages when the cell is isopotential over the distance between the electrodes.

Single-electrode techniques

Modern amplifiers allow measuring voltage with the same electrode that passes current, and most reported traces in the modern literature are obtained from single-electrode recordings. The idea is simply to subtract the estimated pipette voltage from the measured voltage. An example is shown on Figure 3.3B (bottom). One subtracts $R_e^* I$ from the measured trace (Fig. 3.3B, middle), where R_e^* is the estimated electrode resistance. This technique is called *bridge balance* or *series compensation*. The main difficulty is to obtain that estimate. In older amplifiers, this was done by eye: estimated resistance is increased until the trace "looks right". Digital amplifiers can do this estimation automatically, but the procedure is not fundamentally different; essentially, it consists in fitting a model of the response to the measurement (for example a sum of exponentials). Thus there is some imprecision in the estimation of R_e. Additionally, there is also a capacitive current through the pipette wall and at the amplifier, and therefore applying bridge balance results in the appearance of capacitance transients in the trace (Fig. 3.3B, bottom). Amplifiers generally include a *capacitance neutralization* circuit, which consists in injecting a negative capacitive current $-C.dV/dt$. This circuit reduces but does not suppress capacitive transients. As it is a feedback circuit, it can also be unstable and increase noise. There are a few alternative techniques for dealing with electrode artifacts, such as discontinuous current-clamp (DCC), where current injection and voltage measurement are performed in alternation at high rate (Brennecke and Lindemann, 1974), and active electrode compensation (AEC), where a non-parametric model of the electrode is used to estimate electrode voltage (Brette et al., 2008). These are reviewed in (Brette and Destexhe, 2012). None of these techniques guarantees perfect estimation of the intracellular potential.

At the end of 1970s, Neher and Sakmann developed a collection of techniques called *patch clamp* (Neher and Sakmann, 1976; Sigworth and Neher, 1980) (Fig. 3.4). Patch clamp uses glass pipettes with a larger tip, of order 1 μm. Sucb pipettes are not sharp enough to penetrate cells. Instead, the pipette is brought into contact with the membrane and a small suction is applied. The glass then forms a high-resistance seal with the membrane (> 1 GΩ). This is the *cell-attached* configuration, which is used record to currents through the small patch of membrane

[2]The *liquid junction potential* is due to differences in electrolyte compositions and can be calculated, but there is also a tip potential at the cell/electrode interface when the tip is very thin, and this potential is difficult to predict (Purves, 1981).

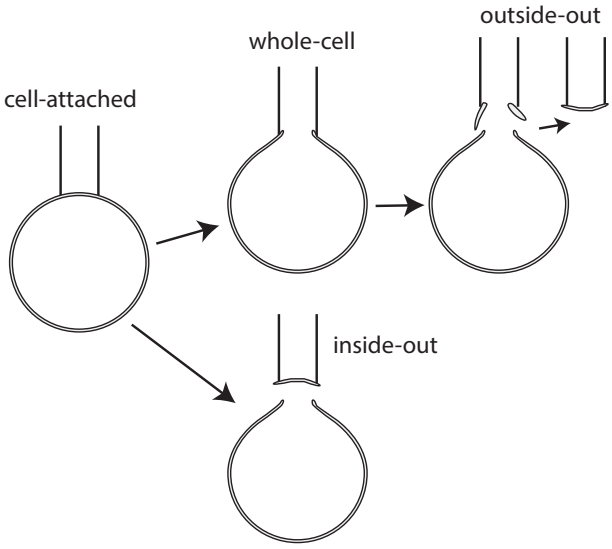

Figure 3.4: Patch-clamp technique with different configurations.

under the pipette. By applying a strong suction, the membrane is ruptured and the pipette is then in contact with the intracellular medium. This is the *whole-cell* configuration. It is used in the same way as sharp microelectrodes, with the additional advantage that pipette resistance is much lower and there is no leak due to the microeletrode piercing the membrane. A disadvantage, however, is that the electrolyte in the pipette diffuses into the cell and eventually replaces it (since it has a much larger volume). Therefore, the pipette solution has to be carefully prepared and in any case intracellular pathways are highly disrupted. A variation of the technique has been introduced to deal with this issue, the *perforated patch*, where the pipette contains antibiotics and is brought in cell-attached mode. The antibiotics progressively forms pores into the membrane, giving electrical access (with higher resistance) without making the membrane permeable to large molecules. The initial motivation of patch-clamp was in fact not to record the intracellular potential of a cell but rather to record transmembrane currents through ionic channels. This can be done in two ways. The first way is to bring the pipette in cell-attached configuration then pull it, bringing with it a small patch of membrane. This is the *inside-out* configuration. The second way is to bring the pipette in whole-cell configuration then pull it, bringing with it a small disrupted patch of membrane that reseals, with the outside now facing the extracellular medium. This is the *outside-out* configuration. With the patch clamp technique, it is possible to record currents flowing through a single channel (see section **??**). In any case, patch-clamp, as all other techniques, is not ideal since the intracellular medium is not preserved (except for perforated patch, which has higher access resistance). It is also not universal, and in particular it cannot be used in an intact Paramecium, because of the cilia and inner membranes.

Current clamp and voltage clamp

The configuration when we record the voltage response of the membrane to a current, as shown for example on Figure 3.3, is called *current clamp*. Current clamp is not appropriate to measure the current-voltage relationships of different ionic channels. The first reason is that the membrane has a capacitance that produces a current $C.dV/dt$ (C is membrane capacitance) when

the membrane potential varies, and therefore the current flowing through the membrane does not equal the current passing through the electrode. To suppress the capacitive current, the membrane potential must be constant. The second reason is that to measure voltage-dependent changes of permeability, one wants to precisely control voltage. For these two reasons, in the 1940s Marmont and Cole designed the *voltage clamp* technique (Marmont, 1949; Cole, 1949), where the current necessary to maintain the membrane potential at a given value is measured. The basic principle is a feedback system: current is injected when the potential deviates from the target value. In its simplest form: $I = g(V_c - V_m)$, where V_c is the command potential (target), V_m is the measured membrane potential and g is a large feedback gain. If the gain is large enough, then $V_m \approx V_c$ and I is recorded. When the membrane potential is clamped, the electrode current exactly matches the membrane current flowing in the opposite direction. Modern amplifiers use additional techniques borrowed from control theory (Astrm and Murray, 2008).

As for current clamp, electrode resistance poses an issue for single-electrode voltage clamp. The feedback system ensures that the amplifier end of the electrode is clamped at the command potential V_c. However, if a current I passes through the electrode to maintain that potential, then the actual membrane potential is not V_c but $V_c + R_e I$, where R_e is the electrode resistance (more precisely, access resistance as it typically increases when accessing the intracellular medium). Compensation methods are used to deal with this issue, but they do not entirely solve the problem. We can see that the issue is particularly important when measuring large currents, as for example the Na^+ currents responsible for AP initiation. For this reason, in the two experimental preparations that we are going to study in this chapter, two electrodes were used for voltage clamp: one to pass current and another one to measure voltage (Figs 3.1 and 3.2).

There are a number of variations around current clamp and voltage clamp. One is *dynamic clamp*, where the injected current is a function of the measured potential, used in general to mimick ionic currents (Bal and Destexhe, 2009). Another one is *action potential clamp*, where the voltage waveform of an action potential is recorded in current clamp and then used as time-varying command potential in voltage clamp (Carter and Bean, 2009). Optical techniques are also increasingly used to measure the membrane potential and to inject current (Emiliani et al., 2015). However, at the time of writing, these have not reached the level of precision of standard electrophysiological techniques, although they have other advantages, in particular the ability to simultaneous measure membrane potential in the entire cell. Membrane potential can be measured with transmembrane voltage sensors coupled to a fluorescent molecule, which are either injected or genetically expressed. The intensity of the fluorescent signal correlates with membrane potential. The main issues are calibration (mapping optical intensity to membrane potential), noise (high in small structures), response speed and toxicity. Current can be injected by optogenetic techniques, in which a light-sensitive channel is expressed in the membrane. Again calibration and response speed are important issues, because transduced current is not a linear function of light intensity. This chapter will be based mainly on results obtained with standard electrophysiological techniques.

3.2 Passive properties of the isopotential membrane

3.2.1 Resting potential

In chapter **??**, we have seen that membrane polarization is due to ionic concentration gradients across the membrane combined with membrane permeability to specific ions. In the squid giant axon, Hodgkin and Katz showed that the effect of concentration changes on the resting potential were well predicted by GHK theory (**??**), assuming the ratios of membrane permeability to K^+,

		Intracellular concentration (mM)	Extracellular concentration (mM)	E_S (mV)
Squid axon	K^+	410	10	-93
	Na^+	49	460	56
	Cl^-	40	540	-65
Paramecium	K^+	1	40	-92
	Ca^{2+}	10^{-4}	1	230

Table 3.1: Concentrations of the main ions of the cytosol and extracellular medium in the squid giant axon (Hodgkin, 1951), and estimates in Paramecium in a solution with 1 mM KCl and 1 mM $CaCl_2$ (Machemer, 1998), and corresponding Nernst potentials E_S at $T = 20°C$ (see section **??**).

Cl^- and Na^- are around 1:0.45:0.04 (Hodgkin and Katz, 1949). The basis of the resting potential in the squid axon (and other preparations, e.g. the frog muscle) was also confirmed by radioactive tracers, used to measure ionic fluxes at rest (Hodgkin, 1951). The resting potential of the squid giant axon depends on temperature, and is around -60 mV.

In Paramecium, the resting potential is of order -30 mV and it also varies with extracellular ionic concentrations, in particular K^+ and Ca^{2+}. Table 3.1 gives estimated orders of magnitude for intracellular concentrations of K^+ and Ca^{2+} in Paramecium, in a solution with 1 mM KCl and 1 mM $CaCl_2$ (Machemer, 1998). There is normally very little Ca^{2+} inside the cell, perhaps of order 10^{-7} M, as in other cells (including neurons). That concentration rises in the cilia during the action potential. When it exceeds 10^{-6} M, the cilia beat in the reverse direction (Naitoh and Kaneko, 1972).

However, the basis of the resting potential appears more complex in Paramecium than in the squid axon. It varies in complex ways with the concentration of various extracellular cations. Not only does the resting potential vary with extracellular concentrations, but current-voltage relationships appear to shift. This is thought to be due to competitive binding of cations (including Ca^{2+}) to anionic sites on the outer membrane and the development of a surface potential (Eckert and Brehm, 1979). The phenomenon is sketched on Figure 3.5. Paramecium lives in freshwater, where ionic concentrations are much lower than in the sea or in the extracellular space around neurons. The lipids forming the membrane carry negative charges, which produces an electrostatic potential away from the membrane (Fig. 3.5A). Consequently, the membrane potential is smaller than the potential difference measured away from the membrane. When extracellular ionic concentration is high, cations (for example Ca^{2+}) bind to the anionic sites of the membrane, which act as a "screen" for the surface charges (Fig. 3.5B). The membrane potential is then larger. Because the manipulation of extracellular Ca^{2+} concentration (and a number of other cations) shifts the current-voltage relationships, it is thought that the membrane is actually mostly permeable to K^+ at rest and the effect of extracellular Ca^{2+} is mostly on surface potential (i.e., a global shift of the membrane potential). Clearly GHK theory is not sufficient to model current-voltage relationships in this case, but in the following, we will assume that the composition of the extracellular medium is fixed, so we will not deal with these complexities.

3.2.2 Membrane capacitance and resistance

The bilipid membrane is a thin insulator between two conducting media (the electrolytes). Electrically, it behaves as a capacitor, that is, the membrane can store electrical charge by having positively charged particles (in this case, ions) on one side and an equal amount of negatively charged particles one the other side. Charge is proportional to the potential difference between

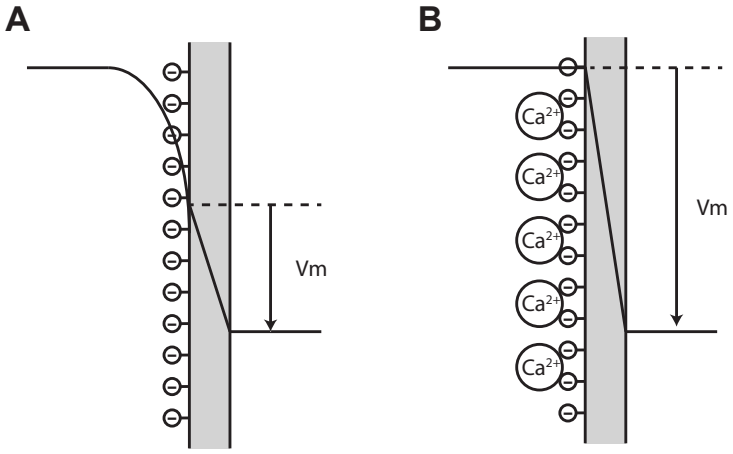

Figure 3.5: Screening of surface charges by extracellular cations in Paramecium membrane (grey). A, In low ionic-strength medium, fixed negative charges on the membrane produce a surface potential, so the potential difference V_m acting on the membrane is smaller than the total potential difference between intra- extracellular medium (the curve represents the potential). B, In high ionic-strength medium, cations (e.g. Ca^{2+}) bind to the anionic sites on the membrane, screening the surface charges, so V_m is larger.

the two sides, and the proportionality coefficient is called *capacitance*. Let us denote Q the total charge on the inner side of the membrane. Then Q and V_m are related by:

$$Q = C.V_m$$

and C is the *membrane capacitance*, expressed in Farad (F). Total charge scales with membrane area, and therefore capacitance also scales with membrane area. Thus membrane capacitance can be written as

$$C = c_m.\text{area}$$

where c_m is called the *specific membrane capacitance* in units of F/m^2. In neurons, $c_m \approx 1$ $\mu\text{F/cm}^2$.

Membrane capacitance can be measured by applying short electrical shocks, i.e., by injecting a short and strong pulse of current through an intracellular electrode. Hodgkin et al. (1952) used the apparatus shown in Fig. 3.1 to apply short shocks of different magnitude on the space-clamped squid giant axon. The total charge Q is the integral of the current: $Q = \int I$, in units of Coulomb (C). In Figure 3.6A, a negative charge was transferred, and we can see that the instantaneous effect on the membrane is a hyperpolarization (V_m becomes more negative) proportional to the charge: $\Delta V_m = Q/C$. In the figure, the charge per unit membrane area $q_m = Q/A$ is reported. Membrane area A was simply calculated as a the area of the cylindrical axon membrane around the part of the electrode exposed to the intracellular medium. We then deduce the specific membrane capacitance: $c_m = q_m/\Delta V_m \approx 0.9$ $\mu\text{F/cm}^2$. The same relation between charge and initial depolarization is seen when positive charges are transferred, but in this case action potentials are triggered (Fig. 3.6B).

This calculation could only be done because the axon was made isopotential. Specific membrane capacitance can generally not be measured in this way in neurons, because a current

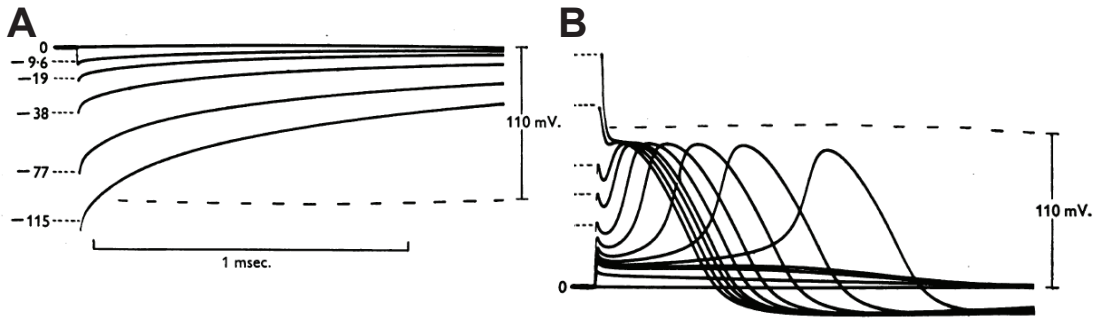

Figure 3.6: Capacitance of the squid giant axon. Short electrical shocks of different magnitudes (total charge in pC/cm^2) are applied to the axon, and the membrane potential is recorded (0 mV means resting potential) (Hodgkin et al., 1952). A, Hyperpolarizing shocks. B, Depolarizing shocks, which trigger action potentials.

injected in the soma does not uniformly depolarize the membrane. Additionally, although it is customary to consider specific membrane capacitance as a biological constant, we must keep in mind that the membrane is crowded and therefore its composition is likely to have some influence on capacitance. The influence of Na channel density on membrane capacitance is considered for example in (Hodgkin, 1975).

After the initial shock, we note in Fig. 3.6A that the membrane potential relaxes to the resting potential. Indeed, when no current is applied through the membrane, we know that the membrane potential stabilizes at a fixed equilibrium value, the resting potential. To understand the dynamics of this relaxation, we need to introduce the concept of *capacitive current*. Suppose an inward (positive) current I is injected through the electrode. Current is the flow of charge; therefore the charge Q increases because of the positive current I: $Q = Q_0 + \int I$ or equivalently $dQ/dt = I$. Using the relation $Q = C.V_m$, we deduce:

$$C.\frac{dV_m}{dt} = I$$

This equation simply expresses conservation of charge, and We call the left handside the *capacitive current* (Fig. 3.7A). It does not correspond to a physical movement of charges through the membrane, but rather it simply expresses conservation of charge. It other words, it describes the redistribution of charges around the membrane due to a transmembrane current. Note that the capacitive current is positive when electrode current I flows inward. Therefore seen as a current "flowing through the capacitor", the capacitive current must be oriented outward, so that outward current equals inward current (conservation of charge).

We can now understand the relaxation of membrane potential towards resting potential after an initial shock. Let $I(V_m)$ be the current-voltage relationship of the membrane (directed inward). Then after the initial shock, we must have:

$$C.\frac{dV_m}{dt} = I(V_m)$$

By definition of the resting potential V_0, we have $I(V_0) = 0$. Around V_0, we can linearize the current-voltage relationship: $I(V_m) \approx g(V_0 - V_m)$, where g is a conductance[3]. The terms *slope*

[3]To find the correct sign, remember that positive ions are pushed in the direction of the electrical field, therefore a positive inward current should be seen when V_m is very negative.

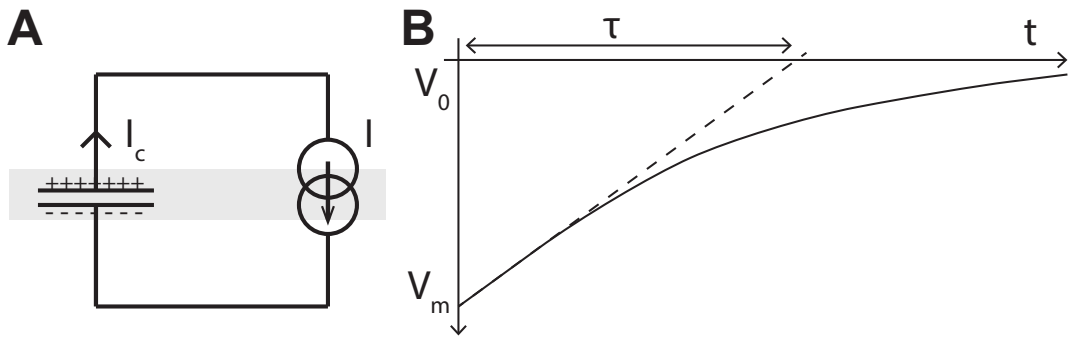

Figure 3.7: Capacitive current. A, The capacitive current $I_c = CdV_m/dt$ represents the redistribution of charge around the membrane induced by the transmembrane current I. B, Exponential decay of membrane potential after an initial electrical shock, with time constant τ.

conductance are sometimes used, as g corresponds to the slope of the current-voltage relationship at V_0. The corresponding resistance $R = 1/g$ is often simply called the *membrane resistance*. This linear current is sometimes called *leak current*. Note however that in the Hodgkin-Huxley model (section 3.4), the current named "leak current" actually corresponds to the unspecific current that remains when K^+ and Na^+ have been discounted.

With this linearization, we obtain the following linear differential equation:

$$C.\frac{dV_m}{dt} = g(V_0 - V_m)$$

This type of equation where the capacitive current is matched to the transmembrane currents is called the *membrane equation*. It is more conveniently expressed in the following form:

$$\tau\frac{dV_m}{dt} = V_0 - V_m$$

where $\tau = RC$ is called the *membrane time constant*. This equation predicts that V_m converges to V_0 (set $dV_m/dt = 0$), and the convergence is exponential:

$$V_m(t) = V_0 + (V_m(0) - V_0)\exp(-t/\tau)$$

The membrane time constant τ can be understood in the following way: if a tangent to the curve is drawn from the initial value after the shock, then the tangent intersects the axis $V_m = V_0$ at time τ (Fig. 3.7B).

Figure 3.8 shows the response of Paramecium to a hyperpolarizing current step (from Machemer and Ogura (1979)). The linearized membrane equation then reads:

$$C\frac{dV_m}{dt} = g(V_0 - V_m) + I$$

where I is the injected current. This equation can be rewritten as above in a more convenient way:

$$\tau\frac{dV_m}{dt} = V_0 - V_m + RI$$

The membrane potential should then converge to $V_\infty = V_0 + RI$ (set $dV_m/dt = 0$). This convergence is exponential with time constant τ:

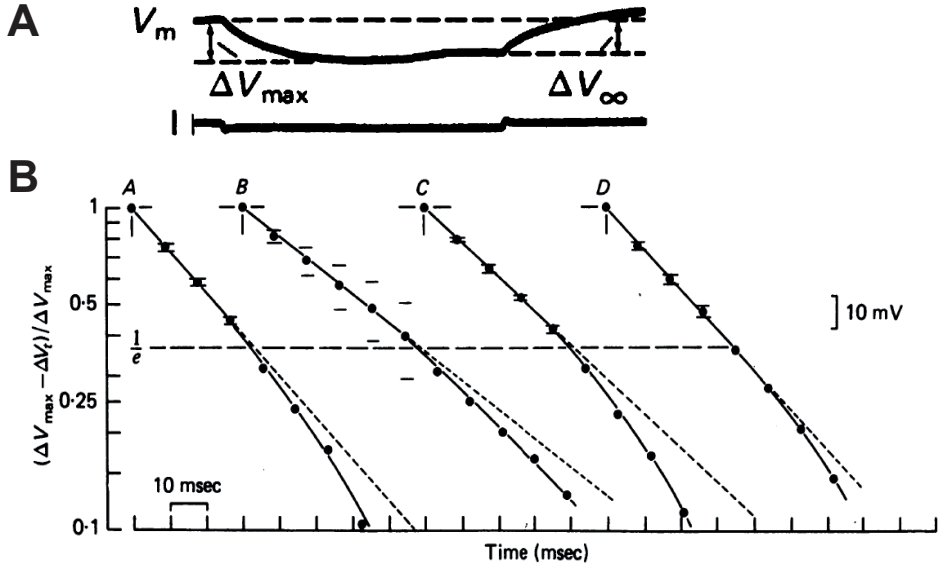

Figure 3.8: Passive response of Paramecium (Machemer and Ogura, 1979). A, Voltage response to a hyperpolarizing current step. B, Normalized relative response in log scale in 4 conditions: non-deciliated (A, B), deciliated (C) and reciliated (D).

$$V_m(t) = V_\infty + (V_m(0) - V_\infty)\exp(-t/\tau)$$

If we choose the equilibrium value V_∞ as the reference potential, that is, if we write $\Delta V(t) = V_m(t) - V_\infty$ (relative hyperpolarization), then we have:

$$\Delta V(t) = \Delta V(0)\exp(-t/\tau)$$

This is perhaps the simplest way to express the solution of a first order linear differential equation: the response relative to the equilibrium value decays exponentially. Figure 3.8B shows $\Delta V/\Delta V_{\max}$ in log scale. According to the formula above, we should see a straight line (oblique dashed line). At time $t = \tau$, we must have $\Delta V(t)/\Delta V(0) = 1/e$. Therefore, we obtain an estimate of τ from the intersection of the experimental curve with the horizontal line $\Delta V(t)/\Delta V(0) = 1/e$ (dashed). For the first experimental curve (A), we find $\tau \approx 35$ ms. The membrane time constant is roughly the same when cilia are removed with ethanol (curve (C)). Since the equilibrium value of V_m is determined by the membrane resistance, the response to a current step can be used to estimate both R and τ, or equivalently R and C. For Paramecium, these estimates are $C \approx 700$ pF and $R \approx 65$ MΩ. When cilia are removed, membrane capacitance is approximately halved, which suggests that the membrane area of cilia is approximately half the total membrane area.

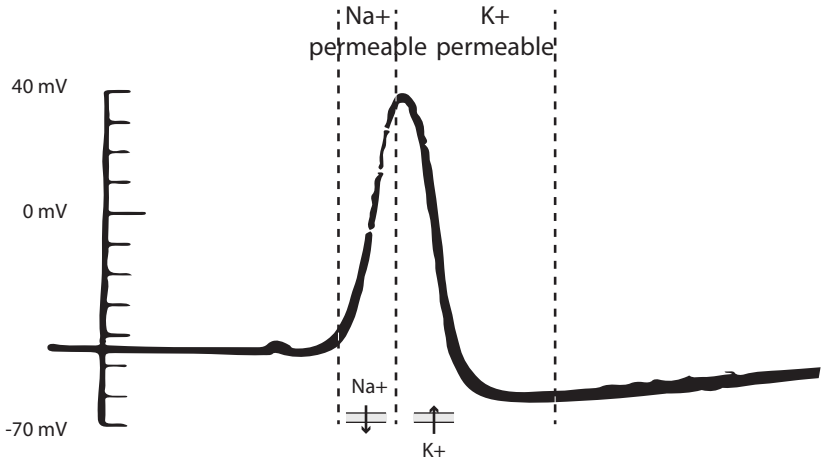

Figure 3.9: Ionic movements and membrane permeability changes underlying the action potential of the squid axon (adapted from (Hodgkin and Huxley, 1939)).

3.3 Active properties

3.3.1 General view

When the membrane potential is depolarized above a certain threshold, an action potential is triggered (Fig. 3.7B). The electrophysiological studies of the 1940s and 1950s converged to the following view of the squid axon's action potential (Figure 3.9). In addition to the passive properties of the membrane responsible for the resting potential, membrane permeability to Na^+ and K^+ changes with membrane potential. In modern terms, there are two types of voltage-dependent ionic channels, specific respectively to Na^+ and K^+. Those channels are closed at rest, but more and more of them open as membrane potential is increased, which increases membrane permeability for specific ions. For example, when an excitable cell is depolarized by an an electrode current, the Na^+ channels first start to open. Because there is more Na^+ outside than inside, Na^+ ions enter the cell, which depolarizes the cell even more. Permeability to Na^+ increases, and therefore even more Na^+ enters: there is a positive feedback, which causes the explosive nature of the AP — we say that the phenomenon is *regenerative*. The membrane potential then approaches the reversal potential of Na^+. Then the Na^+ channels *inactivate*, that is, Na^+ permeability decreases, also through a voltage-dependent process, but slower. Finally K^+ channels open through a slower voltage-dependent process, letting K^+ flow outside the cell, which hyperpolarizes (or "repolarizes") the membrane, towards the reversal potential of K^+. As the membrane potential goes back to its resting value, permeability to the various ions also returns to its resting state.

In Paramecium, the mechanism is similar but varies in detail (Fig. 3.10). The permeability of ciliary membrane to Ca^{2+} increases with membrane potential (and ciliary membrane only (Ogura and Takahashi, 1976)). Because there is much more Ca^{2+} outside than inside the cell, Ca^{2+} flow in when the membrane is depolarized. As for the squid axon, this sets up a positive feedback loop, which produces the explosive, regenerative nature of the action potential, but with a different ionic basis. Calcium APs are seen in other excitable cells, for example the barnacle muscle (Hagiwara et al., 1964), of which there is a classical abstract two-variable mathematical model,

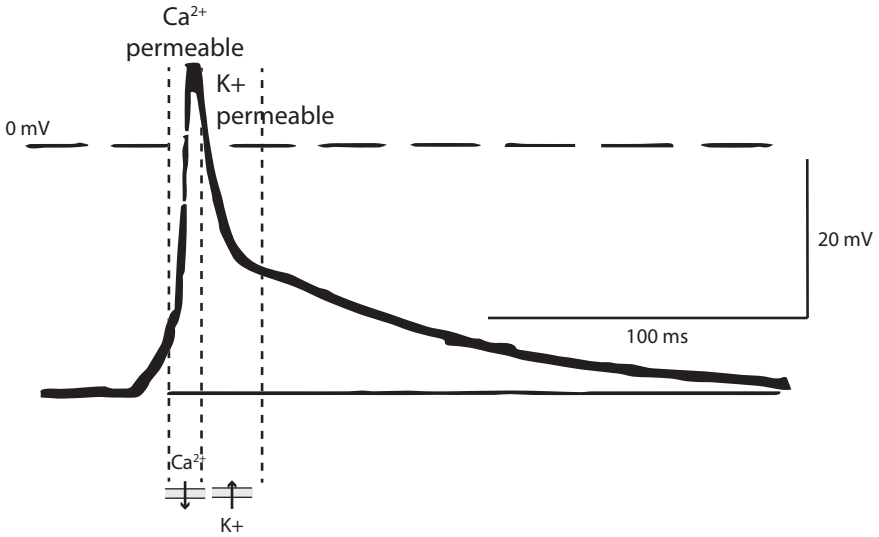

Figure 3.10: Ionic movements and membrane permeability changes underlying the action potential of Paramecium (adapted from (Naitoh and Eckert, 1973)).

the Morris-Lecar model (Morris and Lecar, 1981). Calcium channels also exist and are very important in neurons, but they make a small contribution to the generation of action potentials — rather, they are involved in intracellular signaling pathways, in particular activity-dependent regulation.

Near the peak of the Paramecium's AP, calcium channels also inactivate, i.e., they are not permeable to Ca^{2+} anymore. However, a big difference with the squid axon's AP is that Ca^{2+} channel inactivation is not directly voltage-dependent. Instead, it is the increase in intracellular concentration of Ca^{2+} in the cilia (Brehm and Eckert, 1978) that blocks the channels. This inactivation occurs indirectly through the binding of Ca^{2+} with calmodulin (Saimi and Kung, 1994), an ubiquitous protein that can be a part of the ionic channel, and is also found in neurons (Peterson et al., 1999). The permeability to K^+ also increases with membrane potential, but more slowly. As in the squid axon, this increase is responsible for a fast repolarization of the membrane. There are also K^+ channels that are activated by intracellular calcium (Eckert and Brehm, 1979).

There are substantial differences between Paramecium and the squid axon action potentials, but the main ingredients are the same: 1) membrane currents caused by selective changes in membrane permeability; 2) a positive feedback loop in the depolarization; 3) delayed inactivation and repolarization. We now examine some of the empirical basis of this general view.

3.3.2 Membrane impedance during the action potential

As we have mentioned in chapter **??**, one early theory about excitability, proposed by Bernstein, was that the action potential is due to a non-selective increase in membrane permeability. To test this hypothesis, Cole and Curtis measured the time course of the transverse impedance of the membrane during the action potential. This was first performed in Nitella, an alga (Cole and Curtis, 1938), and shortly after in the squid giant axon (Cole and Curtis, 1939). The method uses two extracellular electrodes placed on opposite sides of the membrane (Fig. **??**A

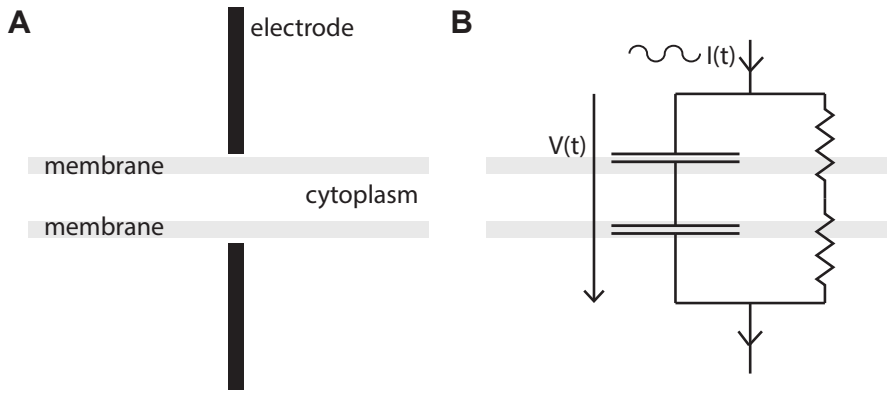

Figure 3.11: Transverse impedance measurement of the squid axon. A, Two extracellular electrodes are placed on opposite sides of the axon. B, Equivalent electrical circuit: sinusoidal current $I(t)$ is passed through one electrode and collected at the other; potential difference $V(t)$ is measured.

and 3.11A). An alternating current $I(t)$ of frequency f is passed through one electrode and the potential difference $V(t)$ between the two electrodes is measured. When there is no current, there should be no potential difference between the two electrodes. If the current I passed through the electrodes is small enough, then the voltage V should depend linearly on I. Using the principle of frequency decomposition, each frequency component of $I(t)$ should be mapped to the same frequency component for $V(t)$, with a different amplitude and phase. In the complex domain, we write:

$$I(t) = I_0 e^{2i\pi ft}$$

and the voltage is then

$$V(t) = I_0 Z(f) e^{2i\pi ft}$$

where $Z(f)$ is a complex number, depending on frequency, called the *impedance*. In practice, for a sinusoidal current, one measures the gain G (ratio of amplitudes of V over I) and the phase difference ϕ, and the impedance is $Z(f) = Ge^{i\phi}$. This number can be related to the membrane capacitance and the membrane resistance. Assume first that the current-voltage relationship of the membrane is linear, with conductance g and resting potential V_0, and note V_i the intracellular potential and V_1 and V_2 the two electrode potentials. The current I passes through electrode 1, enters the cell on one side, leaves the cell on the other side and passes through electrode 2. The equality of the currents entering and exiting the cell means:

$$I(t) = -C\frac{d(V_i - V_1)}{dt} - g(V_i - V_1 - V_0) = C\frac{d(V_i - V_2)}{dt} + g(V_i - V_2 - V_0)$$

We then sum the two expressions and with $V = V_2 - V_1$ we obtain:

$$2I(t) = -C\frac{dV}{dt} - gV$$

The notable fact is that the resting potential V_0 disappears from the equation, so the response is equivalent to that of an electrical circuit with a capacitance and resistance in parallel (Fig.

3.11B). Let us calculate the impedance. We simply replace $I(t)$ and $V(t)$ by the complex expressions above and after simplifications we obtain:

$$2 = (-2i\pi fC - g)Z(f)$$

Thus if we measure the impedance $Z(f)$, then we can deduce the membrane capacitance and conductance (specifically, $g = \mathrm{Re}(-2/Z(f))$). This method can be applied if the non-stationary case of an action potential. If at a given instant t the instantaneous current-voltage relationship of the membrane is linear (as in the Hodgkin-Huxley model, see section 3.4), then we can simply replace g by $g(t)$ and V_0 by $V_0(t)$. We then apply the measurement on a short time window where $g(t)$ and $V_0(t)$ do not change much and use a high frequency current $I(t)$. We then obtain $g(t)$, the total membrane conductance at that particular moment — we are assuming that the current is small enough so that it does not perturb the cell. Figure **??**A (right) shows the time course of the membrane conductance (fast oscillating trace) superimposed on the action potential of the squid axon: the membrane conductance increases dramatically during the action potential. This is in line with Bernstein's theory, according to which membrane permeability increases during the action potential.

Nonlinear current-voltage relationships

As we have mentioned several times, the current-voltage relationship of the membrane is often not linear. Nevertheless, the measurement is still meaningful in this case. Let us consider that the membrane current is $f(V_m, t)$, a function of both membrane potential and time. Then the equality of currents entering and leaving the cell means:

$$I(t) = -C\frac{d(V_i - V_1)}{dt} - f(V_i - V_1, t) = C\frac{d(V_i - V_2)}{dt} + f(V_i - V_2, t)$$

If the current I is small, then so is $V = V_2 - V_1$. Therefore, adding the two expressions gives:

$$2I(t) \approx -C\frac{dV}{dt} - \frac{\partial f}{\partial V}(V_i - V_1, t)V$$

The quantity $\partial f/\partial V$ is called the *slope conductance*, it is the local membrane conductance at particular the membrane potential and time. This is the quantity measured by the transverse impedance measurement technique. It quantifies the effect of a small perturbation of membrane potential on membrane current. In the case of the GHK current model, for example, it is proportional to membrane permeability, assuming ionic concentrations are constant.

3.3.3 Ionic basis of the action potential

The measurements of Cole and Curtis showed that membrane conductance increases during the action potential, in agreement with Bernstein's theory. Shortly after these studies, in 1939, Hodgkin and Huxley made the first intracellular recording of the squid axon action potential, which clearly demonstrated that the membrane potential transiently becomes positive (Hodgkin and Huxley, 1939) (Fig. **??**C). This observation contradicts Bernstein's hypothesis that the action potential is due to a non-specific increase in membrane permeability, because this would result in an action potential peaking near 0 mV. A different theory emerged: the rising phase of the AP is due to an increase in Na^+ permeability, while the falling phase is due to an increase in K^+ permeability. The basic observations that supported this theory, reviewed in (Hodgkin, 1951), are as follows:

- Ionic fluxes for specific species can be measured with radioactive tracers. These measurements revealed an influx of Na^+ and outflux of K^+ during electrical activity. Today similar measurements can be done using with fluorescent probes[4], for example for Na^+, which show increases in intracellular Na^+ concentration associated with APs (Kole et al., 2008; Fleidervish et al., 2010; Baranauskas et al., 2013). A quantitative argument can be made: the amount of Na^+ entering the cell during an AP should be at least as large as the amount necessary to charge the membrane capacitance towards the peak of the AP[5]. This amount of charge can be calculated as explained in section **??**. Measurements of Na^+ flux with radioactive tracers showed indeed that the influx was 2-3 times larger than the minimum value. Measurements of K^+ flux showed that the outflux of K^+ was similar to the influx of Na^+, as expected from electroneutrality.

- Manipulation of Na^+ concentration: when sodium is removed from the extracellular medium, action potentials disappear. This observation was in fact made very early by Overton (1902) in frog muscle, and then repeated in other preparations including the squid axon. In addition, when extracellular Na^+ concentration is decreased, the peak value of the action potential decreases (Fig. 3.12A). At high concentration, the variation agrees with the Nernst potential of Na^+ (solid line).

- The duration of the action potential is very short, on the order of 1 ms (see Fig. **??**C). If the falling phase were due to only to the membrane permeability returning to its resting state, then we would expect the membrane potential to decay more or less exponentially with the same time constant as in response to small shocks near rest (Fig. 3.7). The fact that the membrane potential returns to rest very quickly indicates that K^+ permeability is much higher during the falling phase than at rest.

- After the falling phase, the membrane potential goes beyond the resting potential, towards the Nernst potential of K^+ (Fig. **??**C). Again this indicates strong membrane permeability to K^+.

Similar experimental observations have been done in vertebrate neurons (see e.g. Fig. 3.12B). In Paramecium, the membrane potential also changes sign at the peak of the action potential (Fig. 3.10), and the peak value varies with extracellular Ca^{2+} concentration, while extracellular K^+ concentration has small impact (Fig. 3.12C,D). On Fig. 3.10, it can also be noted that the falling phase is faster than expected from passive properties (Fig. 3.8), which indicates that K^+ permeability increases after the action potential peak. In Paramecium, action potentials are graded: their amplitude depends on the stimulating current. Graded APs are converted to all-or-none APs when calcium is partly replaced by barium (Ba^{2+}) in the extracellular solution (Naitoh and Eckert, 1968), or when EGTA is injected intracellularly. Calcium channels are permeable to barium, which competes with Ca^{2+}, while EGTA binds with calcium and thus lowers intracellular concentration of Ca^{2+} (Brehm et al., 1978). These and other experimental observations have led to the following conclusions: Ca^{2+} concentration increases in the cilia during the rising phase of the AP, and this increase inactivates Ca^{2+} channels (Eckert and Chad, 1984) and activates K^+ channels; there are also K^+ channels that are activated by depolarization as in the squid axon. Thus the mechanism of repolarization is quite different in the squid axon and in Paramecium, since in Paramecium it is mostly intracellular Ca^{2+} and not membrane potential that controls it.

[4]The general principle is that the fluorescent properties of the probe depends on whether it is bound with the target intracellular ion (ion specificity depends on the probe), so that the fluorescent signal can be related to the ion concentration.

[5]It could be larger since Na^+ influx could occur concurrently with K^+ outflux.

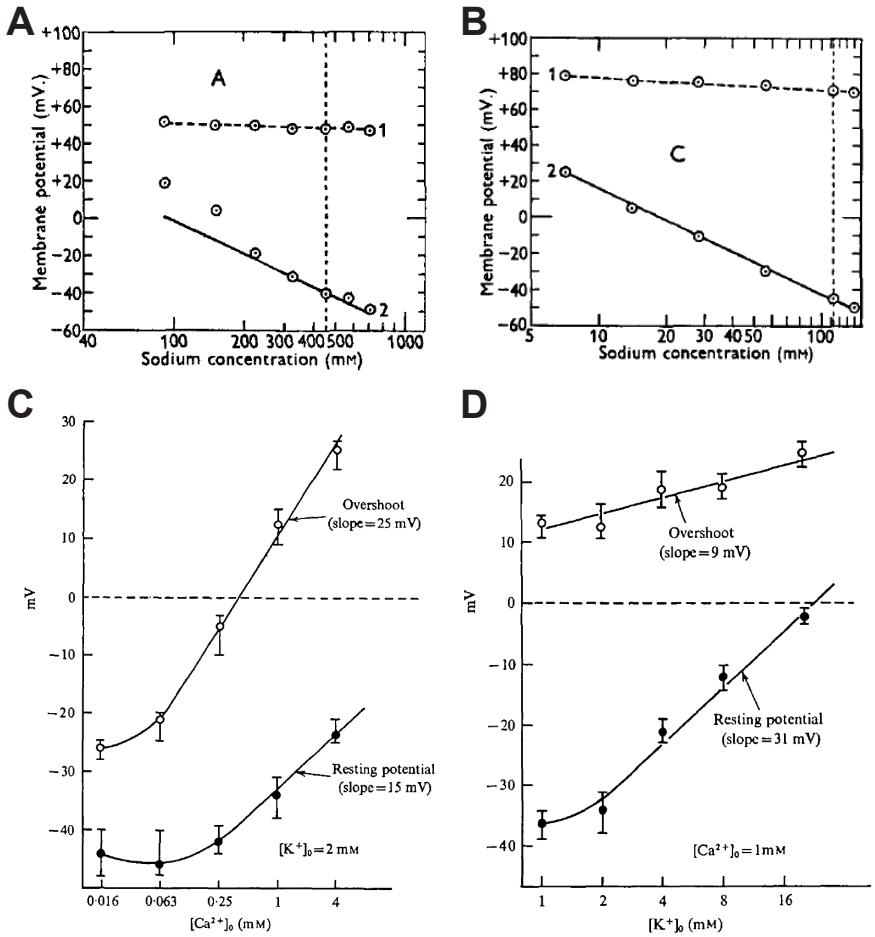

Figure 3.12: Effect of ionic concentrations on action potentials. A, Resting potential (1, top) and peak of action potential (2, bottom) as a function of extracellular Na^+ concentration in the squid axon (Hodgkin, 1951). The difference between extracellular and intracellular potential is plotted (i.e., $-V_m$). B, Same as A in frog myelinated fiber. C, Same as A in Paramecium, except extracellular Ca^{2+} concentration is varied (Naitoh et al., 1972). The convention for potential is reversed (V_m is plotted). D, Same as C except extracellular K^+ concentration is varied.

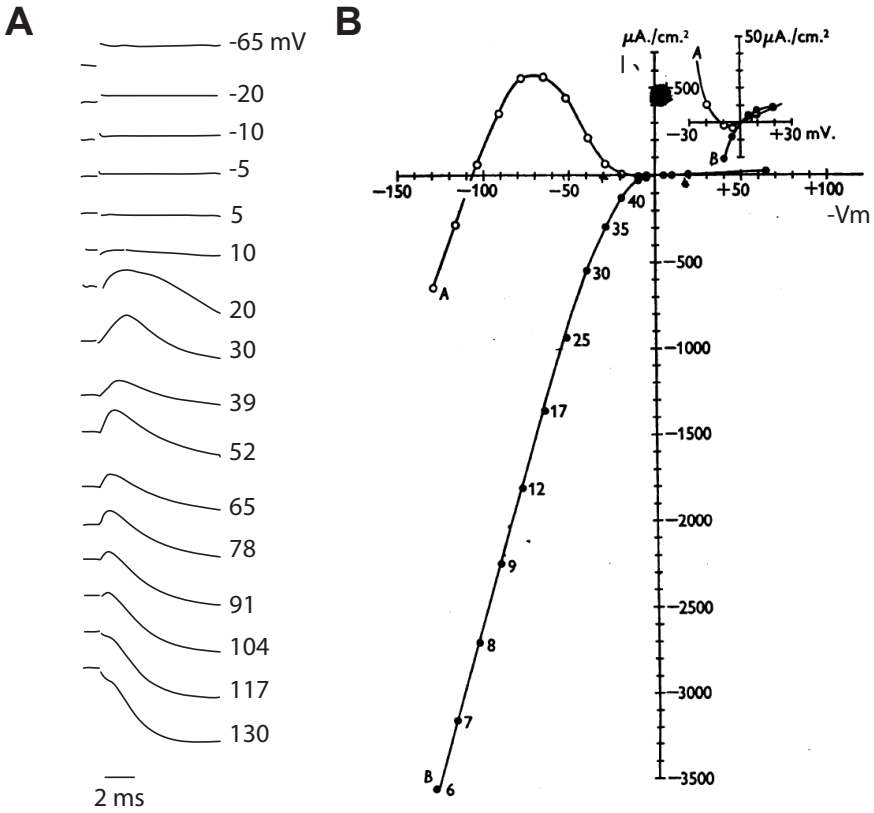

Figure 3.13: Membrane current of the squid axon recorded in voltage-clamp (adapted from Hodgkin et al. (1952)). A, Currents recorded in voltage-clamp with a step depolarization to the value of V_m indicated on the right, relative to resting potential. Positive current means inward. Capacitive transients were subtracted. B, Current vs. $-V_m$ measured 0.63 ms after the voltage step (open circles) and in steady-state (filled circles).

3.3.4 Dynamics of membrane currents

Dynamics of the total membrane current

As we have pointed out in section 3.1, the key technique to investigate the dynamics of membrane permeability is voltage-clamp: the current required to maintain the membrane potential at a fixed value is measured. There are several reasons. The first is technical: the capacitive current $C.dV_m/dt$ is null when the membrane potential is constant and therefore the electrode current matches the membrane current. But this is a relatively minor issue because the capacitive current could in principle be calculated and subtracted from the measurement. The second reason is that when the membrane potential is constant, the temporal variations of the membrane current reflect changes in permeability, if we assume that ionic concentrations do not vary significantly. This is true both of the linear (ohmic) model of membrane currents and of GHK theory (section **??**). The third reason is that one needs to control the membrane potential in order to investigate the voltage-dependent properties of membrane permeability.

Results of a voltage-clamp experiment in the squid axon are shown on Fig. 3.13A, where

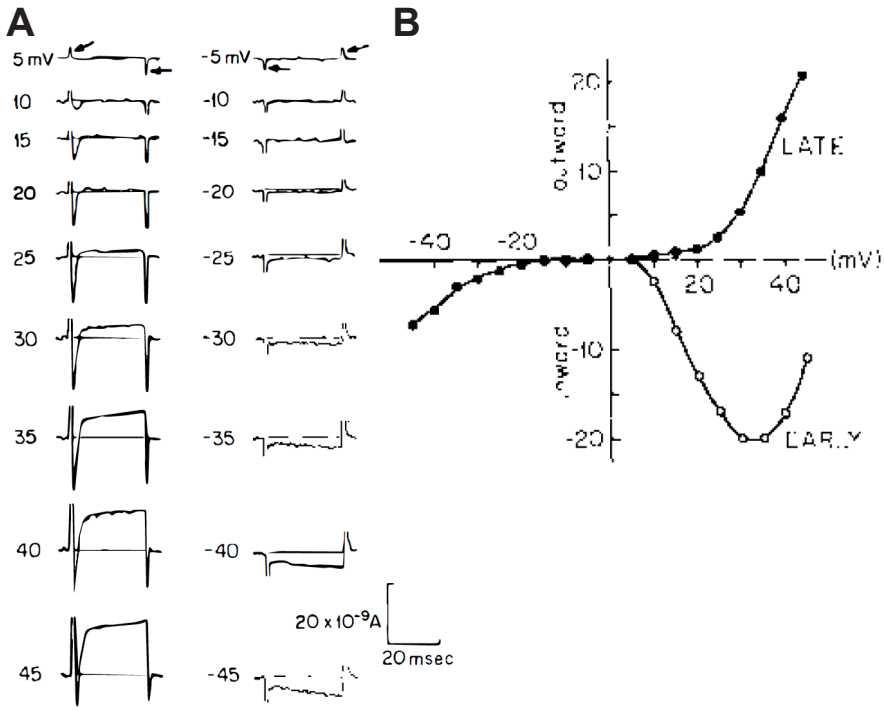

Figure 3.14: Membrane current of Paramecium recorded in voltage-clamp (Eckert and Brehm, 1979)). A, Currents recorded in voltage-clamp with a step depolarization. Negative current means inward. Capacitive transient are seen at the beginning and end of the voltage step (arrows). B, Current vs. V_m measured at the peak (open circles) and 30 ms after the voltage step (filled circles) (note the opposite convention for both voltage and current compared to Fig. 3.13B).

voltage is instantaneously switched from resting potential to a target value. In the hyperpolarized range, the current switches to a different value and stays constant. When the target voltage is 20 mV above resting potential or more, the current increases then decreases and changes sign: first it is inward, consistent with positive ions entering the cell (possibly Na^+), then it is outward, consistent with positive ions leaving the cell (possibly K^+). At very depolarized voltages, above E_{Na}, the current is outward. On Figure 3.13B, we observe that the early current (here at 0.63 ms) is non-monotonous and reverses around 100 mV. This suggests that the early current is due to Na^+ permeability increasing with membrane potential (note that $-V_m$ is on the horizontal axis). The late current (steady-state value) reverses at the resting potential and the voltage-dependence is much steeper at depolarized voltages. This suggests that the late current is due to K^+ permeability increasing with membrane potential, but more slowly than Na^+ permeability. Similar observations can be made on Paramecium (Fig. 3.14; note the opposite conventions for current and voltage).

Separation of ionic currents in the squid axon

To understand these currents in terms of changes of Na^+ and K^+ permeabilities (or Ca^{2+} and K^+ for Paramecium), one needs to isolate the currents carried by each of these ion species. The method used by Hodgkin and Huxley was to measure the membrane current in voltage-clamp with different extracellular Na^+ concentrations. To that effect, sodium was partly or entirely replaced by choline in the extracellular medium, to which the membrane is not permeable (Hodgkin and Huxley, 1952c). Entirely replacing sodium by choline makes the axon completely inexcitable with almost no change in the resting potential.

Let us consider two extracellular solutions with different Na^+ concentration. Assuming the K^+ current is not affected Na^+ concentration (which is approximately but not exactly true), the currents recorded in voltage-clamp are $I = I_{Na} + I_K$ and $I' = I'_{Na} + I_K$, that is, only the Na^+ current should differ between the two traces. Therefore the difference $I - I' = I_{Na} - I'_{Na}$ is only due to the Na^+ current. The Na^+ current is the time-dependent permeability of the membrane times a factor that depends on membrane potential and ionic concentrations (e.g. in the GHK model, section **??**). Since the membrane potential is fixed, it follows that the two currents I_{Na} and I'_{Na} are proportional: $I_{Na} = kI'_{Na}$. Therefore, $I - I' = (1 - k)I_{Na}$. The proportionality constant k can be deduced by assuming that initially $I \approx I_{Na}$ and $I' \approx I'_{Na}$. We can then deduce both I_{Na} and I_K.

An example is shown on Figure 3.15. With this separation technique, we observe that when the axon is depolarized (here by 56 mV above rest), the Na current first increases (inward), reaches a peak, then decreases and returns near its initial value (Fig. 3.15B). As pointed out above, this means that the membrane first becomes permeable to Na^+, then impermeable again. The first process is called *activation* and the second *inactivation*. The K^+ current does not show inactivation (Fig. 3.15c): an outward current develops and converges to a steady-state. We also note that the activation of the K^+ current is slower than that of the Na^+ current. The inactivation of the Na^+ current is voltage-dependent. To demonstrate it, Hodgkin and Huxley used more complex voltage-clamp protocols, where the membrane potential is first clamped to a small depolarized value V_1 for a variable duration, then clamped to a larger depolarized value V_2 (Fig. 3.16A). With $V_1 = 8$ mV and $V_2 = 44$ mV above resting potential, the inward current is only seen in response to the second voltage step, but its amplitude depends on the duration of the first step — the longer the first step, the smaller the inward current in response to the second step. Since there is no measurable current in response to the first step, the inactivation is unlikely due to ionic movements but rather voltage-dependent. The voltage-dependence can be measured by varying the value V_1: the relative amplitude of the inward current decreases as V_1

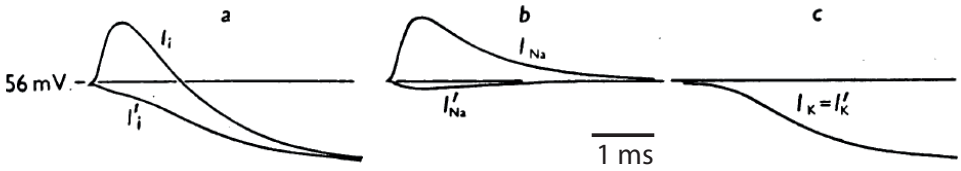

Figure 3.15: Separation of membrane currents in the squid axon (Hodgkin and Huxley, 1952c). The membrane potential is stepped from resting potential to 56 mV above it, in two experimental configurations: in sea water (I_i, I_{Na}, I_K), and in sea water with lowered sodium concentration (10%). (a) Total membrane current ($I > 0$ means inward current). (b) Sodium current. (c) Potassium current.

is increased (Fig. 3.16B; remember potential is given with the inverse convention extracellular minus intracellular potential $= -V_m$).

To interpret these currents in terms of permeability changes, Hodgkin and Huxley define the *chord conductance* as the current divided by the driving force. For example, for Na^+, the chord conductance is $I_{Na}/(V_m - E_{Na})$. This is a definition that can always be made, independently of whether the instantaneous relation between membrane current and driving force is linear — but of course, it is more meaningful in that case, which turns out to be approximately the case in the squid axon in normal physiological conditions. Figure 3.17 shows the dynamics of Na^+ and K^+ conductances when the axon is depolarized to various membrane potential values. The general time course of the conductances is of course similar as that of the ionic currents, but additionally we note that the maximum conductance increases monotonously with membrane potential, for both Na^+ and K^+.

These experimental observations form the basis of the Hodgkin-Huxley model of the action potential of the squid axon (section 3.4). Separation of ionic currents is now typically done in a different way, using pharmacological blockers. These are molecules that bind selectively to certain ionic channels and block them. For example, tetrodoxin (TTX) is a toxin produced by some fish, which blocks a large class of Na channels when applied extracellularly (Narahashi et al., 1964). There are many other blockers, for different types of ionic channels, which bind either on the extracellular or intracellular side of the membrane. The effect of blocking Na channels is similar to removing Na^+ is the extracellular medium, but not exactly equivalent, because the ionic selectivity of channels is not perfect (for example, some calcium can pass through Na^+ channels (Baker et al., 1971)). This topic will be discussed further when we introduce ionic channels in chapter **??**.

Separation of ionic currents in Paramecium

In Paramecium, the separation technique used by Hodgkin and Huxley is unfortunately not effective. In addition to the dependence of surface charges on extracellular Ca^{2+} concentration that we have previously discussed (section 3.1), part of the K^+ current is activated not by voltage but by intracellular Ca^{2+}. Besides, the Ca^{2+} current is inactivated not by voltage but also by intracellular Ca^{2+}. Therefore, when extracellular Ca^{2+} concentration is manipulated, the Ca^{2+} current changes in a nonlinear way (because inactivation is modified) and the K^+ current is also affected.

Therefore, alternative techniques have been used in Paramecium. First, cesium (Cs) and tetraethylammonium (TEA) block a large class of K^+ channels (mostly when intracellular in-

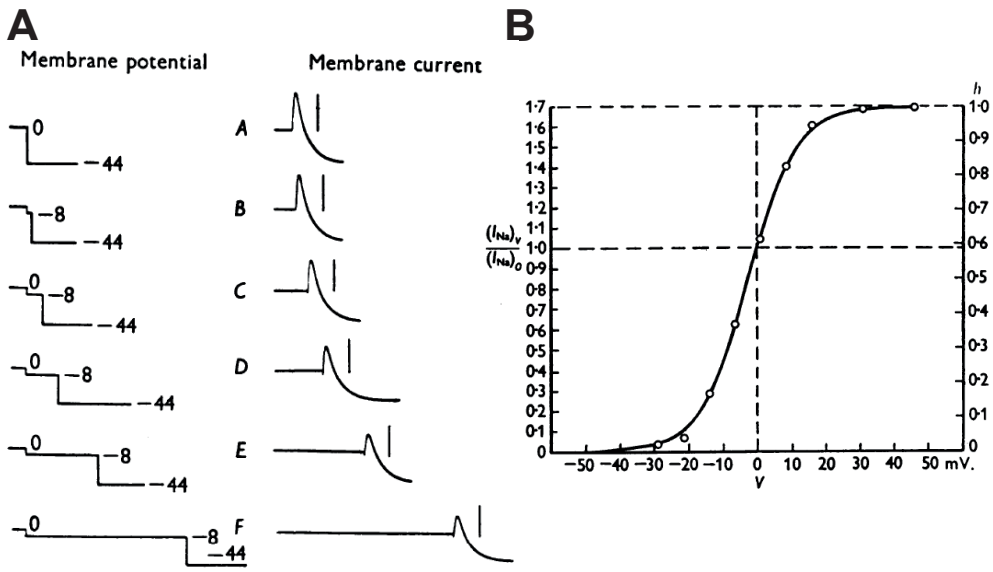

Figure 3.16: Inactivation of the Na^+ current in squid axon (Hodgkin and Huxley, 1952d). A, Two-step voltage-clamp protocol: membrane potential is first depolarized by $V_1 = 8$ mV for variable duration, then by 44 mV above resting potential. Note that potentials are given with the convention $V = V_e - V_i = -V_m$. B, Relative amplitude of the inward current for initial steps of long duration, as a function of V_1.

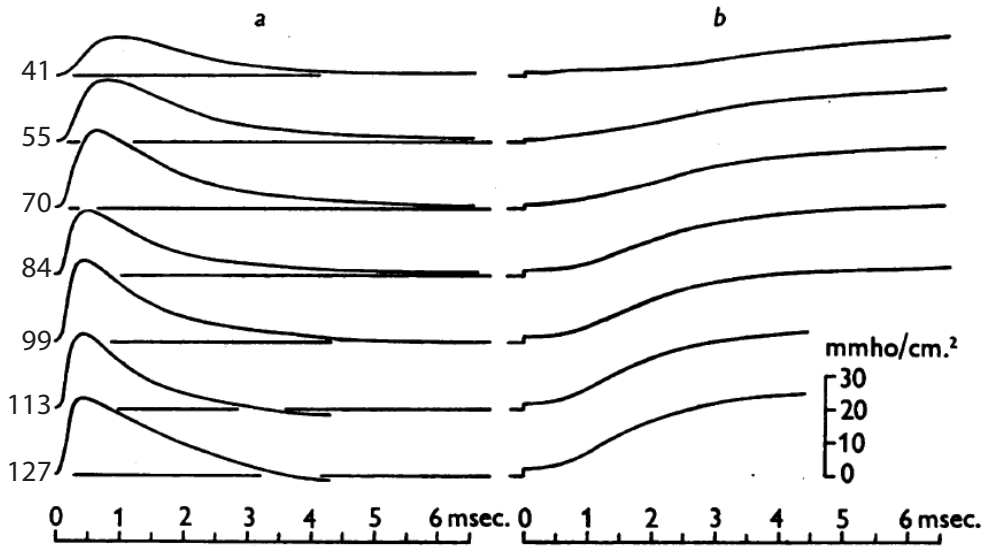

Figure 3.17: Ionic conductances of the squid axon (Hodgkin and Huxley, 1952c). Dynamics of Na^+ (a) and K^+ (b) chord conductances when the membrane potential is displaced from rest to a depolarized value (in mV on the left, relative to resting potential).

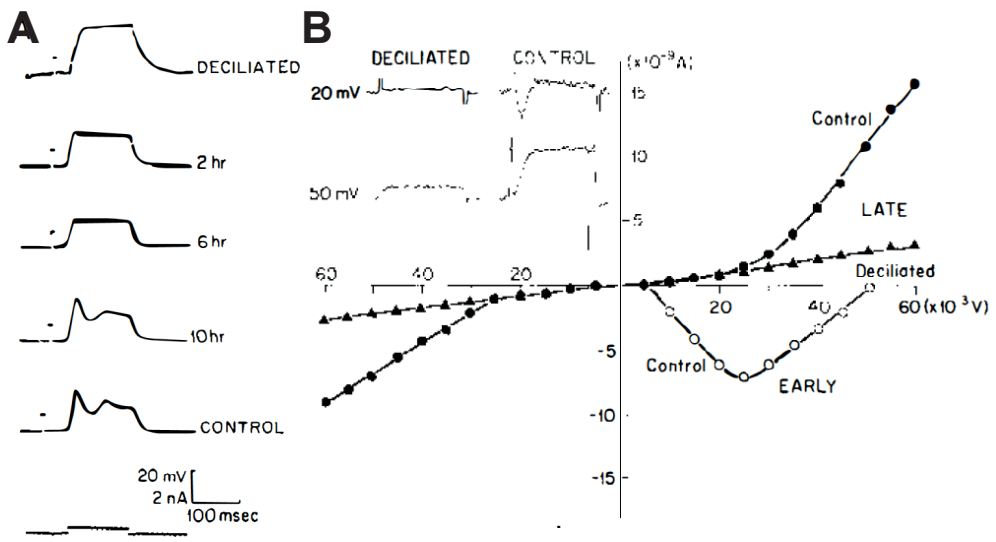

Figure 3.18: Effect of deciliation on the membrane current of Paramecium (Eckert and Brehm, 1979). A, Current-clamp response to a current pulse just after deciliation (top) and several hours after deciliation (below). B, Membrane current measured in voltage-clamp in control (disks) and deciliated (triangles) Paramecium as a function of membrane potential (relative to resting potential). For the control Paramecium, early and late (30 ms) currents are shown (they are identical for the deciliated Paramecium).

jected), and their application nearly suppresses the late outward current but not the early inward current shown in Fig. 3.14B (Brehm et al., 1978). Calcium channels can be blocked by W-7 (Hennessey and Kung, 1984). Another method uses physical separation of channels. As discussed in section 3.2.2, ionic channels are spatially segregated, with Ca^2+ and K^+ channels responsible for the action potential located in the cilia. Figure 3.18 shows the effect of deciliation on voltage responses to current pulses (A) and on current measured in voltage-clamp (B). Both the early inward current and the late outward current disappear when cilia are removed. After a few hours, the cilia grow back and the cell becomes excitable again, which makes Paramecium an interesting model of development of excitability.

Deciliation does not allow fine separation of ionic currents. Another approach is genetic manipulation. It was used before Ca^+2 channel blockers were identified (Hennessey and Kung, 1984). Paramecium is easy to culture and because there is a direct relationship between electrical activity and behavior, various types of mutants can be isolated on the basis of abnormal behavior, in direct relation with defects in specific current types (Saimi and Kung, 1987). For example, *Pawn* mutants[6] do not show the typical avoiding reaction, and only swim in straight lines or stop. Electrically, they are not excitable: there is no action potential (Kung and Eckert, 1972) (Fig. 3.19A). This defect can be traced back to a malfunction of calcium channels. When the membrane current is measured in voltage-clamp, it appears that the late (steady-state) current is the same in wild type and mutant Paramecium, but the early inward current is only seen in the wild type (Oertel et al., 1977) (Fig. 3.19B). One can then calculate the difference between membrane currents in wild type Paramecium and Pawn (Fig. 3.19C), which can be shown to

[6]named after the chess piece because they cannot swim backward.

be indeed carried by Ca^{2+}. It then appears that, as in the squid axon, this inward current inactivates rapidly (here a few ms), while the outward current (carried by K^+) does not. The inactivation is apparently nearly complete, but not entirely because ciliary reversal is observed during sustained depolarization. Using two voltage pulses separated by various durations, it can be shown with this separation technique that inactivation is removed in about 80 ms (Oertel et al., 1977). However, compared to the use of drugs or manipulation of ionic concentrations, genetic separation of ionic currents is based on the comparison between different cells, which is an important limitation since cells vary in the expression and properties of ionic channels.

Unlike the squid axon, inactivation of the inward current of Paramecium is not voltage-dependent but calcium-dependent (Brehm and Eckert, 1978; Brehm et al., 1978, 1980; Eckert and Chad, 1984). This can be demonstrated by different means reviewed in (Eckert and Chad, 1984). For example, when extracellular Ca^{2+} is partially replaced by barium (Ba^{2+}), an early inward current can still be measured upon depolarization in voltage-clamp, but its decay is much slower (Brehm and Eckert, 1978). In current-clamp, this manipulation makes Paramecium produce all-or-none action potentials, with duration increasing with Ba^{2+} concentration (Naitoh and Eckert, 1968). This is consistent with the calcium channel being also permeable to Ba^{2+}, and inactivation due to the intracellular increase in Ca^{2+}. When the membrane current is measured in voltage-clamp in response to two voltage pulses separated by a few tens of ms, the peak inward current is smaller in response to the second pulse, and its relative amplitude decreases as extracellular Ca^{2+} concentration increases (Brehm et al., 1980). Finally, a calcium chelator called EGTA can be injected into the cell. It binds to Ca^{2+} and thereby reduces its intracellular concentration. When this is done in Paramecium, inactivation is much reduced, as measured by the double-pulse method (Brehm et al., 1980).

As shown in Fig. 3.19B, the outward current measured at 25 ms is essentially the same in wild-type Paramecium and in the Pawn mutant with defective Ca^{2+} channels. This and other observations indicate that the outward current measured on this time scale is not triggered by the entry of Ca^{2+} but by depolarization, as in the squid axon. On longer time scales (100-1000 ms), another type of K^+ current develops, activated by intracellular Ca^{2+}, but it is not involved in generating of the action potential (Oertel et al., 1977; Satow and Kung, 1976; Satow, 1978; Satow and Kung, 1980).

3.3.5 Refractoriness

Once an excitable cell has produced an action potential, it is more difficult to excite again for a short period of time. That is, a stronger stimulus is required to make the cell fire another action potential. This is called the *refractory period*. One may distinguish the absolute refractory period, when the cell is not excitable at all, and the relative refractory period, when it is excitable with a stronger stimulus. There are two causes of refractoriness: the inward current (Na^+ for the squid axon, Ca^{2+} for Paramecium) inactivates and therefore is smaller when a second stimulus is applied; an outward current (K^+) develops when a first stimulus is applied, which reduces the effect of a second stimulus and competes with the inward current.

An example in shown in Figure 3.20A in Paramecium. When the cell is stimulated by two current pulses separated by several hundred ms, the same action potential is produced. When the interpulse interval is reduced, a smaller action potential is seen; if it is reduced further, the regenerative component disappears and only a passive response to the stimulus is seen. The reduction in the depolarization by the stimulus (non-regenerative) is due to the outward current, but the complete loss of excitability is due to the inactivation of the inward current (Na^+ or Ca^{2+}). We have seen that inactivation is responsible for the decay of the inward current underlying the action potential, as seen in voltage-clamp (e.g. Fig. 3.17a). Both in Paramecium

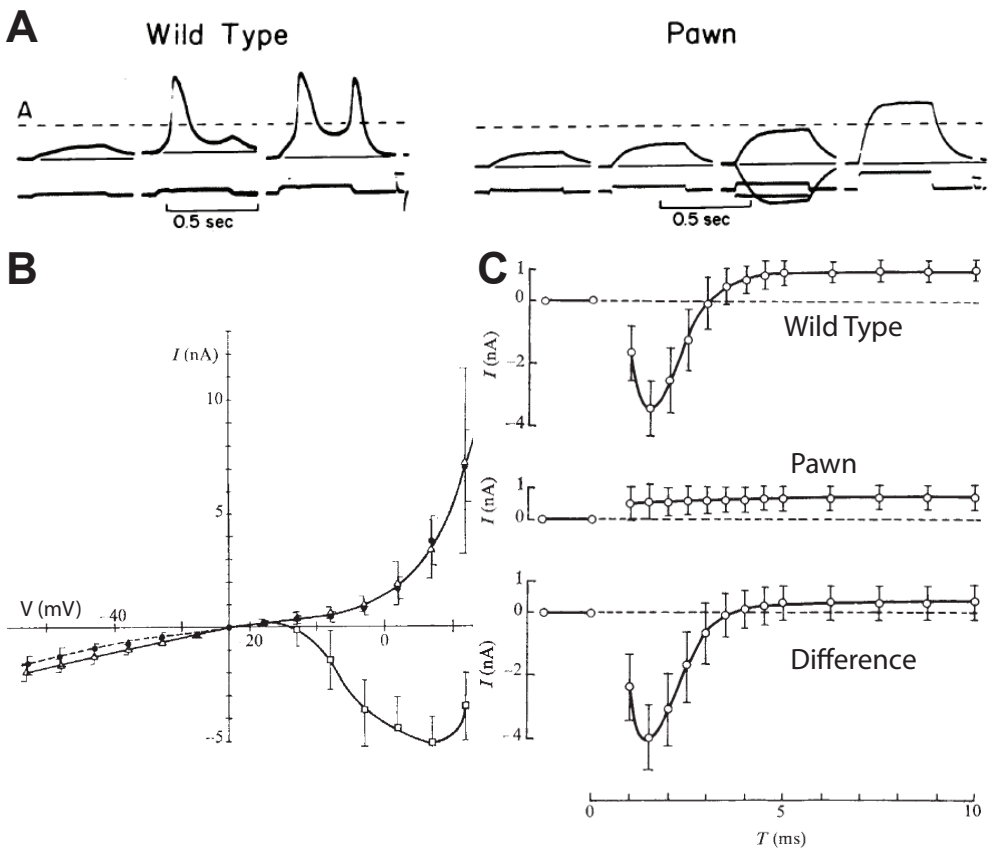

Figure 3.19: Genetic separation of ionic currents in Paramecium. A, Response to current steps in wild-type Paramecium and Pawn mutant (Kung and Eckert, 1972). B, Early current in wild type Paramecium (squares) vs. membrane potential, and late current wild type (triangles) and mutant Paramecium (disks) (Oertel et al., 1977). C, Membrane current measured in voltage-clamp with a 20 mV depolarization in wild type (top) and mutant (middle) Paramecium, and difference between the two current waveforms (bottom) (Oertel et al., 1977).

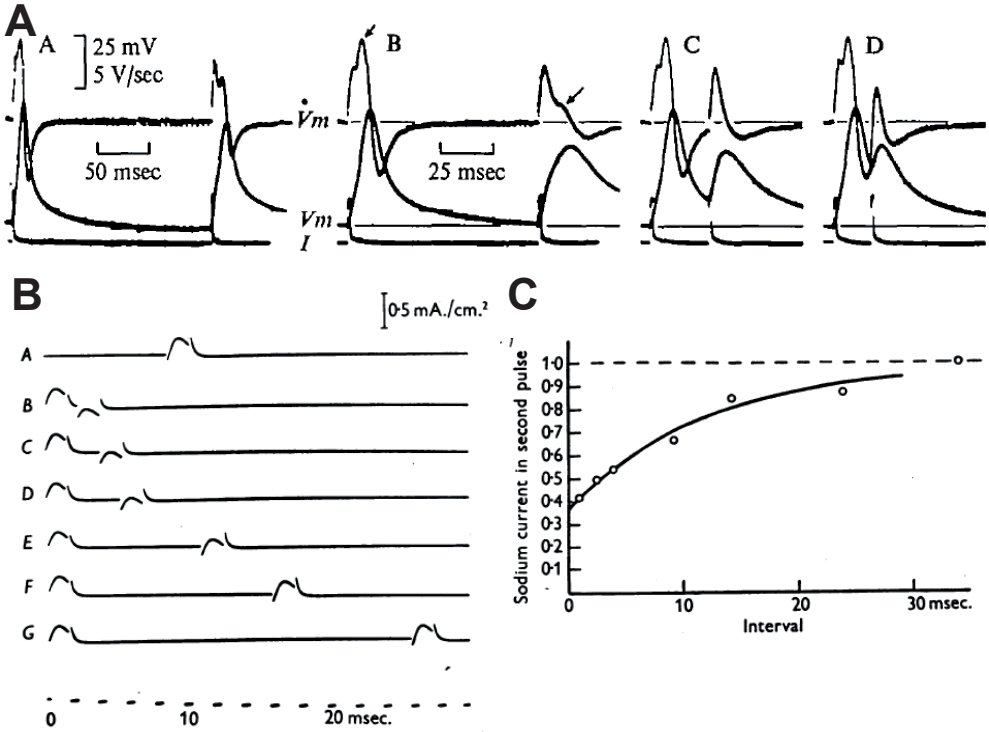

Figure 3.20: Refractoriness of excitable cells. A, Two short current pulses (2 ms) are injected in Paramecium with varying interpulse interval (Naitoh et al., 1972). Membrane potential (bottom) and its derivative (top) are shown. The arrows point a second peak in dV_m/dt corresponding to the inward Ca^{2+} current. B, Current recorded in voltage-clamp for two 44 mV voltage pulses with varying interpulse interval (Hodgkin and Huxley, 1952d); inward current (Na^+) is positive (note that there are also capacitive transients). Top trace: response to a single pulse. C, Relative peak current in the second pulse as a function of interpulse interval.

and in the squid axon, inactivation actually persists much longer than the action potential. This is shown for the squid axon in Fig. 3.20B, where the current is recorded in voltage-clamp in response to two 44 mV voltage pulses lasting about 2 ms (Hodgkin and Huxley, 1952d). Each voltage pulse triggers an inward current, but the amplitude of the current in response to the second pulse is reduced if the interval between two pulses is shorter than about 20 ms — much longer than the duration of the action potential. Figure 3.20C shows that the inward current is reduced by about 60% after an action potential, and then recovers approximately exponentially with a time constant of about 12 ms.

3.4 The Hodgkin-Huxley model

The series of experiments done by Hodgkin and Huxley on the space-clamped squid axon culminated in the design of a quantitative model of the action potential, now called the Hodgkin-Huxley model (Hodgkin and Huxley, 1952a). There is one quantitative model of Paramecium action potential that reproduces some of its qualitative features (Hook and Hildebrand, 1979), but it is

less tightly bound to experimental data. The complete model is presented in section 3.4.4, but as we also want to explain how the model was built, we will introduce its ingredients one by one, together with the corresponding hypotheses and experiments.

3.4.1 The equivalent circuit

First, the membrane is considered isopotential, that is, the membrane potential V_m is the same everywhere. This assumption does not hold in any neuron, except possibly in developing neurons that do not have neurites[7]. As discussed in section 3.1, the assumption holds for the experiments of Hodgkin and Huxley because a metal wire is inserted inside the axon, but this is not the physiological condition (unlike in Paramecium). The Hodgkin-Huxley model is thus a model of the action potential of the space-clamped squid giant axon.

Second, the total membrane current is modelled as a sum of a Na^+ current I_{Na}, a K^+ current I_K, a non-specific "leak" current I_L carried by Cl^- and other ions (i.e., what remains when the two other ionic currents have been removed), and a capacitive current $C.dV_m/dt$. At first sight this may seem obvious, but it is a hypothesis that the currents carried by different ionic species are independent. It is a logical assumption to make if the Na^+ and K^+ currents are thought to be carried by two physically separate types of ionic channels, each being specific for only one ionic species, but of course this was only a hypothesis. The independence of ionic currents was consistent with the experiments where ionic concentrations are manipulated. In an experiment where a current I is passed through an intracellular electrode, conservation of charge then implies:

$$C\frac{dV_m}{dt} + I_{Na} + I_K + I_L = I$$

This equation is called the *membrane equation*. Here we have adopted the following convention: for the electrode current, $I > 0$ means positive current is injected into the cell (inward); for the ionic currents, $I_{Na} > 0$ means current is leaving the cell (outward). This is the modern convention, but Hodgkin and Huxley used the opposite convention. This equation corresponds to an equivalent electrical circuit with different elements in parallel: a capacitor and several sources of current.

3.4.2 The linear model of currents

In section 3.3.4, we have seen that Hodgkin and Huxley introduced the *conductance* g_S of the membrane for a given ion species S, defined by the formula

$$I_S = g_S(V_m - E_S)$$

where I_S is the current (e.g. Na^+ current) and E_S is the reversal potential for S. At this point, this is just a definition, called the *chord conductance*, which can be used whether the current-voltage relationship of the membrane is linear or not. For example, one could define the chord conductance for a membrane with fixed permeability governed by GHK theory, where the current-voltage relation is nonlinear (section **??**). In that case, the conductance would be a function of permeability but also of membrane potential, which makes the definition less useful. The basic postulate of the Hodgkin-Huxley model is that chord conductances depend only on permeability and not on instantaneous voltage. As we have seen in the previous section, membrane permeability can change with membrane potential, but not instantaneously. Therefore

[7]Even in that case, there can be spatial gradients of membrane potential across the cell, i.e., electrical fields within the cell, see for example De Loof (1986) and Levin (2014).

this linear or *ohmic* model consists in separating the ionic current in two factors, one called the driving force ($V_m - E_S$), which is a linear instantaneous function of V_m, and another one, the conductance g_S, which may vary with V_m but not instantaneously.

To test this hypothesis experimentally is straightforward: activate the current with a first voltage-clamp step, then instantaneously move V_m to a different value with a second voltage-clamp step. The current recorded at the beginning of the second step should depend linearly on the imposed voltage. This prediction turns out to be correct for the squid axon, as shown on Figure 3.21 (Hodgkin and Huxley, 1952b). As we have seen before, the peak inward current elicited by a depolarizing voltage step is a nonlinear function of voltage (current I_1, nonlinear curve with crosses). In contrast, the current at the start of a second voltage step depends linearly on voltage, as predicted by the ohmic model (current I_2, linear curve with open disks). The same type of experiments, but with extracellular Na^+ replaced by choline, showed that the K^+ current also follows the ohmic model. However, later experimental studies showed that the current-voltage relationship of the K^+ current is better explained by GHK theory (Clay, 1991, 2005). In some cases such as the Ranvier node of frog myelinated fibers, it was shown that the current-voltage relation of the Na current is also better captured by the GHK current equation (Dodge and Frankenhaeuser, 1959); in the squid axon, the Na current is also nonlinear in low Na water (Hodgkin and Huxley, 1952b). These empirical tests are in fact rarely done and it is often simply assumed that currents follow the ohmic model. A technical difficulty with Na^+ currents is that they have fast kinetics, and the initial response to a voltage step may be unreliable because of the capacitive transient (as seen e.g. on Fig. 3.20B) and incomplete clamp by the amplifier feedback system.

The ohmic model implies that the membrane current associated to ion species S is equivalent to the current of an electrical circuit composed of a battery E_S in series with a resistor of conductance g_S (or resistance $R_S = 1/g_S$) (Figure 3.22). It should be kept in mind that, even when the ohmic model correctly captures the current-voltage characteristics of the ionic current, the conductance still depends on ionic concentrations (and temperature). These concentrations are considered fixed in the Hodgkin-Huxley model, which is justified by the fact that axon diameter is very large (up to 1 mm), so that changes in concentrations due to electrical activity should be very small (see section **??**).

The membrane equation then becomes:

$$C\frac{dV_m}{dt} = g_{Na}(E_{Na} - V_m) + g_K(E_K - V_m) + g_L(E_L - V_m) + I \tag{3.1}$$

3.4.3 Conductance models

The K^+ conductance model

The leak conductance g_L is considered constant. For the K^+ and Na^+ currents, models of the conductances are fitted to voltage-clamp recordings. An example is shown on Fig. for a 25 mV depolarization (A) and the return to (B) resting potential. The conductance increases continuously in some characteristic time (a couple of ms) to a steady-state value, then decreases back to the resting value. The simplest phenomenological model would be an exponential model, that is, where the conductance g_K follows a first-order linear differential equation:

$$\tau\frac{dg_K}{dt} = g_K^\infty - g_K$$

This works well for the deactivation protocol (B), i.e., when the membrane potential is moved back to resting potential, but for the activation protocol (A), it appears that there is a delay in the

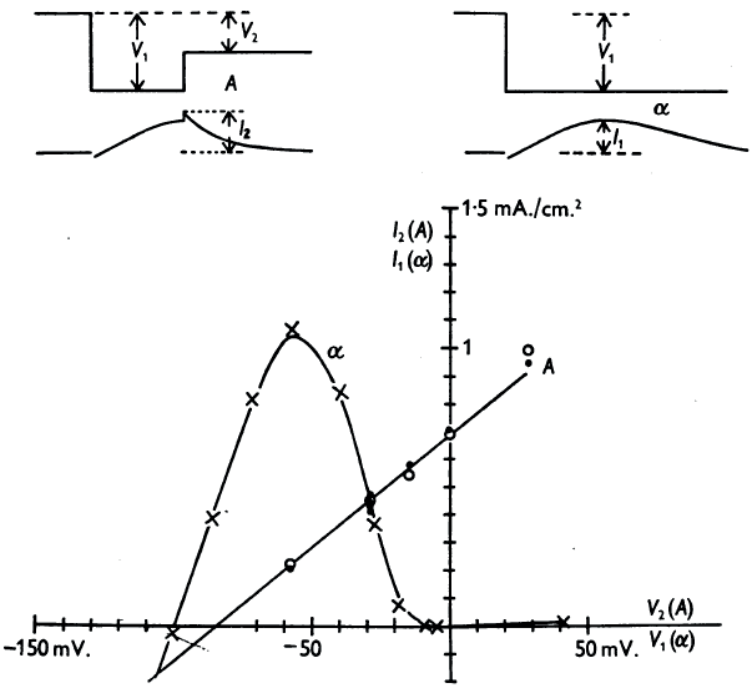

Figure 3.21: Linearity of the Na^+ current-voltage relationship in squid axon, measured in voltage-clamp (Hodgkin and Huxley, 1952b). The nonlinear curve (crosses) represents the peak inward current I_1 measured in a 29 mV depolarizing step (top right) as a function of voltage V_1. The linear curve (open disks) represents the I_2 at the beginning of a second voltage step V_2 (top left). The convention is $I > 0$ for inward current and $V = -V_m$.

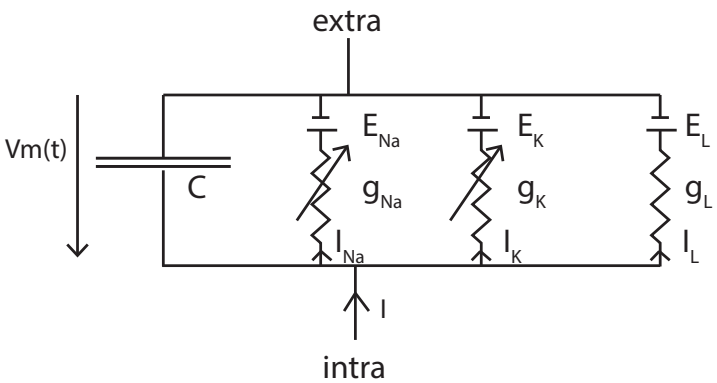

Figure 3.22: Equivalent circuit of the Hodgkin-Huxley model. Each ionic current corresponds to a battery E_S in series with a resistor of variable conductance g_S.

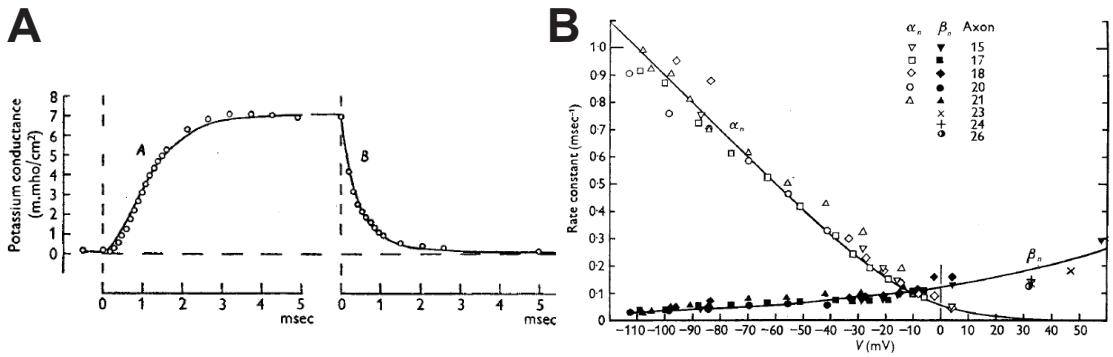

Figure 3.23: Fitting the K^+ conductance of the squid axon (Hodgkin and Huxley, 1952a). A, K^+ conductance measured in voltage-clamp for a 25 mV depolarization and back to resting potential. The curves are fits from the Hodgkin-Huxley model. B, Opening (α_n) and closing (β_n) rates as a function of voltage (convention: $V = -V_m$). The data are collected for different axons and adjusted for temperature.

increase of the conductance, which cannot be obtained with an exponential model. Hodgkin and Huxley then proposed a simple modification, where g_K is proportional to a power of a variable obeying a first-order equation, and found out that an exponent of 4 gave a good empirical fit[8]. The model is then:

$$g_K = \bar{g}_K n^4 \tag{3.2}$$
$$\tau_n \frac{dn}{dt} = n_\infty - n$$

where $\bar{g}_K$ is the maximum conductance and n is a variable between 0 and 1, called *activation variable*; τ_n is the time constant and n_∞ is the steady-state value. The continuous curves in Fig. 3.23A are the fits of this model to the experimental data.

This model can be given the following physical interpretation, which will be elaborated in chapter **??**. K^+ ions can pass through specific ionic channels in the membrane. Each of these channel is made of 4 identical and independent molecules, which can be in two configurations, open and closed, and the channel is open when the 4 molecules are open. A molecule switches stochastically between these two configurations with a transition rate that depends on membrane potential, which can be explained by postulating that the molecules are charged. This is summarized by the following kinetic scheme:

$$\mathrm{C} \underset{\beta_n}{\overset{\alpha_n}{\rightleftharpoons}} \mathrm{O}$$

where C and O represent the closed and open state of a molecule, respectively, α_n is the opening rate and β_n is the closing rate (in s^{-1}). This notation means that a closed molecule has probability $\alpha_n.dt$ of opening in time dt, and an open molecule has probability $\beta_n.dt$ of closing. Then the probability n that the molecule is in the open state follows the following equation:

$$\frac{dn}{dt} = \alpha_n(1-n) - \beta_n n \tag{3.3}$$

[8]Not the best one, however, as a sixth exponent gave a better fit but was considered not worth the extra computing cost, given the machines of the time.

Indeed, the probability $n(t + dt)$ that the molecule will be in the open state at time $t + dt$ is the probability $1 - n(t)$ that it was closed at time t times the probability that it opens in time dt ($\alpha_n.dt$), minus the probability $n(t)$ that it was open times the probability that it closes ($\beta_n.dt$). Opening and closing rates can be given an interpretation in terms of the initial currents measured in the activation and deactivation protocols (Fig. 3.23A). If the channels are initially closed ($n = 0$) and the membrane potential is clamped to a depolarized value, then initially (small t) $n(t) \approx \alpha_n t$ and therefore $g_K \approx \bar{g}_K(\alpha_n t)^4$. The fourth exponent accounts for the "delay" in the current seen in Fig. 3.23A (left), which is scaled by the activation rate α_n. If the channels are initially open ($n = 1$) and the membrane potential is clamped to resting potential, then initially $n(t) \approx 1 - \beta_n t$ and therefore $g_K \approx \bar{g}_K(1 - \beta_n t)^4 \approx \bar{g}_K(1 - 4\beta_n t)$ (Taylor expansion). Thus there is no delay in deactivation, as seen in Fig. 3.23A (right), and the initial rate of decay is proportional to the closing rate β_n.

This kinetic scheme is equivalent to the first-order linear equation above, where

$$n_\infty = \frac{\alpha_n}{\alpha_n + \beta_n}$$
$$\tau_n = \frac{1}{\alpha_n + \beta_n}$$

The fact that the equations provide a good fit to the experimental data of course does not prove that this physical interpretation is correct. In particular, nothing in the experiments of Hodgkin and Huxley indicated the binary and stochastic nature of channel opening (see chapter **??**). In fact, Hodgkin and Huxley did not use term *channel* as it was not at all obvious that ions passed through channels; another hypothesis was that ions cross the membrane by interacting with carriers, an interpretation also consistent with the model (Armstrong, 2007). The Hodgkin-Huxley model is thus better seen as a phenomenological model of membrane permeability rather than a model of ionic channels.

Values of the rates α_n and β_n can then be obtained by fitting conductance measurements from voltage-clamp experiments as shown in Fig. 3.23A, for different values of the membrane potential V_m. Results over a large potential range are shown on Fig. 3.23B, with data collected on a number of axons. These axons were recorded at different temperatures, and temperature has a strong impact on the currents: essentially, it appears that the effect of temperature change is to compress or expand the currents in the time domain[9] (Hodgkin et al., 1952). In the model, this corresponds to scaling the rates α_n and β_n by a constant factor. Empirically, Hodgkin, Huxley and Katz found that the scaling factor to apply is:

$$Q_{10}^{\frac{\Delta T}{10}}$$

where ΔT is the temperature change in degrees (Kelvin or Celsius) and $Q_{10} \approx 3$ in this case. With this correction, there is a clear relation between rates and voltage. These relations were fitted by the following formulae:

$$\alpha_n(V_m) = 0.01\frac{-V_m + 10}{\exp((-V_m + 10)/10) - 1} \tag{3.4}$$

$$\beta_n(V_m) = 0.125\exp(-V_m/80) \tag{3.5}$$

where V_m is in mV and rates are in ms^{-1}. These are empirical formulae, chosen as the simplest mathematical expressions that fit the data; they have no strong biophysical basis. It should

[9]This is of course a rough approximation. Biophysics suggests that the amplitude of the currents should also depend on temperature (see section **??**).

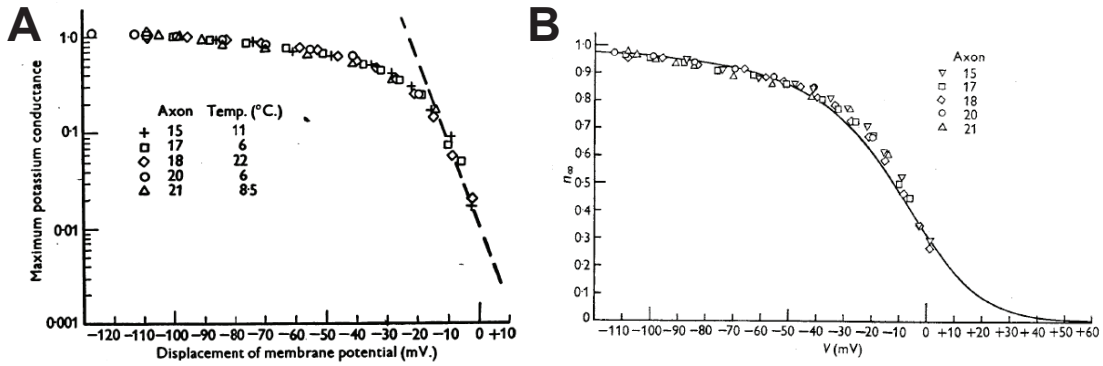

Figure 3.24: The steady-state K^+ conductance of the squid axon. A, Maximum K^+ conductance in log scale vs. voltage ($V = -V_m$) (Hodgkin and Huxley, 1952c). B, Steady-state value $n_\infty(V)$, with the continuous curve representing the Hodgkin-Huxley model of the K^+ conductance (Hodgkin and Huxley, 1952a).

be clear from Figure 3.23B that other choices could have been made, especially for β_n. In particular, an alternative approach would be to fit simple mathematical expressions to n_∞ and τ_n, rather than to α_n and β_n. In electrophysiogical studies, the equilibrium value of the relative conductance ($g_K/\bar{g}_K$), which in the Hodgkin-Huxley model corresponds to $n^4_\infty(V_m)$, is typically fitted to a Boltzmann function of V_m:

$$n^4_\infty(V_m) = \frac{1}{1 + e^{(V_{1/2} - V_m)/k}}$$

where $V_{1/2}$ is called the *half-activation voltage* (value at which $n_\infty = 1/2$) and k is called the *Boltzmann factor* or slope factor. This function has similar shape than the function obtained with equations (3.4) and (3.5) (sigmoidal) but is not identical. In the hyperpolarized range (most channels are closed), this expression predicts:

$$n^4_\infty(V_m) \propto e^{V_m/k}$$

Empirically, Hodgkin and Huxley found indeed an exponential relationship with slope $k \approx 5$ mV (Fig. 3.24A). If $n_\infty(V_m)$ is calculated from equations (3.4) and (3.5), one finds

$$n^4_\infty(V_m) \propto -V_m^4 e^{4V_m/k'}$$

with $k' \approx 9$ mV, i.e., $k'/4 \approx 2.25$, a different relationship. There is indeed some (small) discrepancy between the experimental data for n_∞ and the Hodgkin-Huxley model (Fig. 3.23B).

The Na^+ conductance model

The timecourse of the Na^+ conductance cannot be explained by a first-order linear differential equation, because it is not monotonous (Fig. 3.17A). Therefore Hodkgin and Huxley proposed to model it with two first-order equations, as follows:

$$g_{Na} = \bar{g}_{Na} m^3 h \tag{3.6}$$

$$\frac{dm}{dt} = \alpha_m(1-m) - \beta_m m \tag{3.7}$$

$$\frac{dh}{dt} = \alpha_h(1-h) - \beta_h h \tag{3.8}$$

Equilibrium values (m_∞ and h_∞) and time constants (τ_m and τ_h) are defined as previously as functions of α and β. Another option could have been to model the Na^+ conductance as a second-order equation, but this option was considered simpler. The third exponent (m^3) is empirical. This model can be interpreted as follows: the Na^+ channel (in modern terms) is open when 3 identical molecules are in the same configuration, and when it is not blocked by an additional molecule. We shall call the first kind of molecules the activating molecules and the blocking one the inactivating molecule. Then m is the probability that an activating molecule is in the open state and h is the probability that an inactivating molecule is in the non-blocking state. Again this is just a possible interpretation of the empirical equations, that nothing in the experiments specifically supports — except that the time course of the conductance is well fitted by the model.

In principle, this model could be fitted to current waveforms as for the K^+ conductance. However, in part for technical reasons, Hodgkin and Huxley used a different set of experiments to constrain the inactivation parameters, except for large depolarizations where they assumed $h_\infty = 1$. Specifically, they used the two-step protocol where the peak current in response to a second voltage step is measured (Fig. 3.16). In that protocol, a first step is applied with voltage V_1 and long duration. At the end of the step, according to the model, $m = m_\infty(V_1)$ and $h = h_\infty(V_1)$. If V_1 is small enough, then we can assume $m \approx 0$ (no activation). This is the case represented in Fig. 3.16A where the first step does not trigger any significant inward current. A second step is then applied with high voltage V_2 and the peak current is measured. If V_2 is large enough, then (by assumption) $m_\infty(V_2) = 1$ and $h_\infty(V_2) = 0$. It follows that during the second step:

$$m = 1 - e^{-t/\tau_m(V_2)}$$
$$h = h_\infty(V_1) e^{-t/\tau_h(V_2)}$$

Therefore the current is proportional to $h_\infty(V_1)$. If V_2 is held fixed while V_1 is varied, then the timecourse of the current is not changed, only its amplitude is. It follows that the peak current is indeed proportional to $h_\infty(V_1)$. However, this depends critically on the assumption that V_1 is such that $m_\infty(V_1) \approx 0$, that is, for moderate depolarizations. For larger V_1, not only the amplitude of the current depend on $m_\infty(V_1)$, and not only $h_\infty(V_1)$, but the peak is reached at a time that depends on V_1, i.e., the timecourse of the current is no longer invariant. Therefore this method of measuring h_∞ has a restricted range of applicability.

As for the K^+ conductance, α_h and β_h can be deduced from estimates of h_∞ and τ_h. These estimates are shown on Figure 3.25 for a number of axons; the uncertainty is clearly significant (compare with Fig. 3.23). The rates of activation and inactivation were then fitted to the

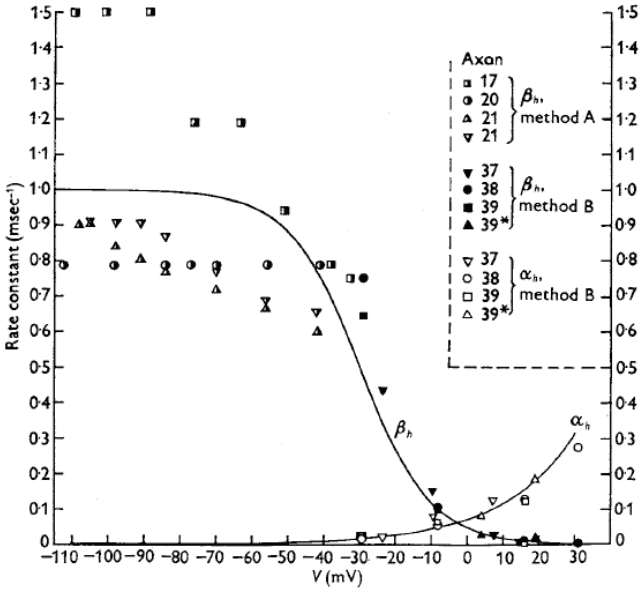

Figure 3.25: Fitting Na^+ inactivation properties of the squid axon (Hodgkin and Huxley, 1952a). Rate constants of inactivation as a function of voltage ($V = -V_m$), estimated in different axons (adjusted for temperature) using a one-step activation protocol (method A) or a two-step inactivation protocol (method B). Smooth curves are model fits.

following formulae:

$$\alpha_m = 0.1\frac{-V_m + 25}{\exp((-V_m + 25)/10) - 1} \tag{3.9}$$

$$\beta_m = 4\exp(-V_m/18) \tag{3.10}$$

$$\alpha_h = 0.07\exp(-V_m/20) \tag{3.11}$$

$$\beta_h = \frac{1}{\exp((-V_m + 30)/10 - 1)} \tag{3.12}$$

This way of calculating *activation curves* ($m_\infty(V)$) and *inactivation curves* ($h_\infty(V)$), based on one-step and two-step protocols, is still widely used in electrophysiology, but mostly to give a general idea of the voltage-dependent properties of ionic channels. Quantitative fitting of models would now be done numerically by using nonlinear fitting techniques, where parameters are automatically adjusted so as to provide the best fit to a set of voltage-clamp measurements (generally in the sense of least squares). Nevertheless, the same one-step and two-step protocols are generally used to produce the experimental data to be fitted.

Constant	Value
C	1 μF/cm^2
E_{Na}	115 mV
E_K	−12 mV
E_L	10.613 mV
g_{Na}	120 mS/cm^2
g_K	36 mS/cm^2
g_L	0.3 mS/cm^2

Table 3.2: Main constants of the Hodgkin-Huxley model.

3.4.4 The full model

Putting equations (3.1)–(3.12) together, we obtain a complete model of the space-clamped squid axon, recapitulated below:

$$
\begin{aligned}
C\frac{dV_m}{dt} &= \bar{g}_{Na}m^3h(E_{Na}-V_m) + \bar{g}_K n^4(E_K - V_m) + g_L(E_L - V_m) + I \\
\frac{dm}{dt} &= \alpha_m(1-m) - \beta_m m \\
\frac{dh}{dt} &= \alpha_h(1-h) - \beta_h h \\
\frac{dn}{dt} &= \alpha_n(1-n) - \beta_n n \\
\alpha_m &= 0.1\frac{-V_m + 25}{\exp((-V_m+25)/10) - 1} \\
\beta_m &= 4\exp(-V_m/18) \\
\alpha_h &= 0.07\exp(-V_m/20) \\
\beta_h &= \frac{1}{\exp((-V_m+30)/10 - 1)} \\
\alpha_n &= 0.01\frac{-V_m + 10}{\exp((-V_m+10)/10) - 1} \\
\beta_n &= 0.125\exp(-V_m/80)
\end{aligned}
$$

where rates are in ms^{-1} and V_m is in mV in the expression of rates. The remaining constants are listed in table 3.2. Conductance densities where obtained from the voltage-clamp measurements discussed previously. Reversal potentials for Na^+ and K^+ were obtained from previous experiments and are relative to the resting potential (i.e., $V_m = 0$ mV means the neuron is at rest). The leak potential E_L is chosen so that the resting potential of the model is 0 mV.

The full model predicts the membrane current measured in voltage-clamp, as well as the membrane potential in current-clamp. A remarkable achievement of this model is that it makes excellent predictions for both sets of experiments with no further optimization. In addition, the model can be readily extended to a model of action potential propagation (by adding the axial current, see chapter **??**), and again with no further optimization, it correctly predicts action potential shape, conduction velocity (to about 20%) and total conductance (as shown in Fig. **??**A). Figure 3.26 shows action potentials produced by the model, compared with measured ones. Some discrepancies are noticeable, for example in the repolarization phase, but otherwise the match is excellent. The model also accounts for Na^+ and K^+ fluxes, subthreshold oscillations and other phenomena.

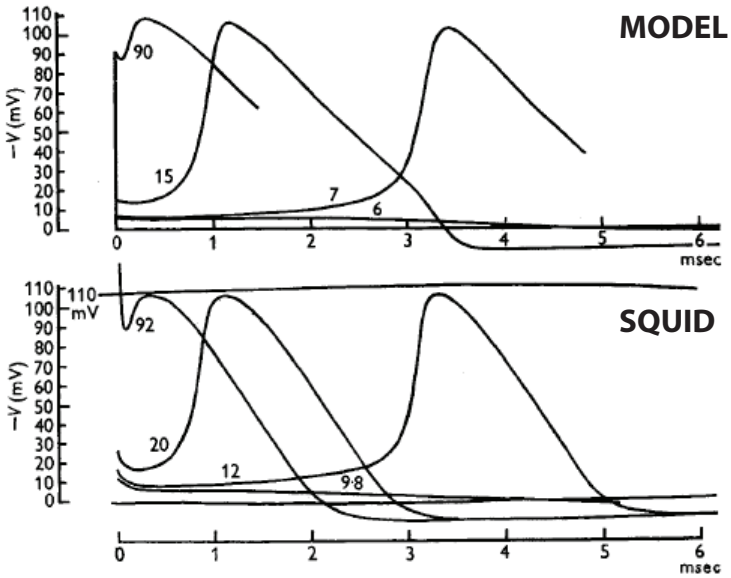

Figure 3.26: Simulated and measured action potential of the space-clamped squid axon (Hodgkin and Huxley, 1952a). Top: action potential of the Hodgkin-Huxley model for different initial depolarizations (numbers in mV). Bottom: measured action potential of the space-clamped squid axon for different initial shocks (numbers in nC/cm^2, correponds to expected initial depolarization in mV).

3.4.5 The squid axon after Hodgkin and Huxley

The Hodgkin-Huxley model was a great achievement, and it turned out that the same formalism could be applied to virtually all excitable cells. The example of Paramecium shows that important modifications can be necessary, for example inactivation of the inward current can depend on the entry of current rather than on voltage. Although the Hodgkin-Huxley model is the historical model of the squid axon action potential, research on this topic continued after 1952. Not surprisingly, a number of modifications have been introduced since then, which are summarized in (Clay, 2005). Here we shall mention a small number of them.

The K^+ current

When discussing their results, Hodgkin and Huxley pointed out that their model of the K^+ current did not fully account for the activation delay seen in voltage-clamp experiments. In the model, this delay is tuned by the exponent 4 in the K^+ current equation (n^4). The reason for choosing that exponent was mainly technical: it was computationally difficult to use larger exponents. Later work showed that an exponent as large as 25 (n^{25}) better accounts for the experimental data (Cole and Moore, 1960).

More fundamentally, the K^+ current actually follows the GHK theory, rather than a linear model (Clay, 1991). In GHK theory, the current is the product of permeability and of a rectifying function of voltage. Using the GHK equation for the K^+ model makes the equilibrium permeability $n_\infty^4(V_m)$ a much steeper function of voltage.

K^+ ions can also accumulate around the axon during the repolarisation phase, which then reduces the K^+ current.

The Na^+ current

In the frog node of Ranvier, it was found that the Na^+ current follows GHK theory, not a linear model (Frankenhaeuser, 1960). One may wonder why it would be linear in the squid axon. This seems to be a serendipitous consequence of the interaction of external Ca^{2+} with Na^+ channels; in calcium-free medium, the Na^+ current of the squid axon does follow the GHK formula (Vandenberg and Bezanilla, 1991a).

Considerable research on Na^+ channels has taken place since the 1950s, and many new models have been proposed, including for the squid axon. These models generally take the form of kinetic models of channels with a number of states and voltage-dependent transition rates (see chapter **??**). They depart from the Hodgkin-Huxley model in several respects, reviewed in (Patlak, 1991) (see Tables 1 and 3 thereof). One is that activation and inactivation are not independent processes (Bezanilla and Armstrong, 1977; Armstrong and Bezanilla, 1977; Vandenberg and Bezanilla, 1991b,a). Rather, several state transitions toward the open state must occur before the channel can be inactivated.

Other currents

Other channels than Na^+ and K^+ channels are known to exist in the squid axon. For example, there are calcium channels that let extracellular calcium ions enter the axon when an action potential is produced (Baker et al., 1971). A different type of Na^+ channels, with distinct electrophysiological properties, has also been found, although it accounts for a small proportion of the current (Gilly and Armstrong, 1984).

3.5 A quick guide to the 1952 Hodgkin-Huxley papers

It is an excellent exercise and introduction to electrophysiology to study the series of 5 papers by Hodgkin, Huxley and Katz published in 1952. In these papers, the electrical conventions are quite different from modern conventions. Membrane potential is relative to rest (i.e. 0 mV at rest). In voltage-clamp results, voltage is the opposite of membrane potential, i.e., extracellular potential minus intracellular potential, and current is oriented from extracellular to intracellular, i.e., $I > 0$ means inward current.

1. Hodgkin, A. L., Huxley, A. F., and Katz, B. (1952). Measurement of current-voltage relations in the membrane of the giant axon of Loligo. *The Journal of Physiology*, 116(4):424–448.

   This paper introduces the space-clamp and voltage-clamp technique, including detailed information about the feedback system of the amplifier. Capacitive currents and membrane currents are presented.

2. Hodgkin, A. L. and Huxley, A. F. (1952). Currents carried by sodium and potassium ions through the membrane of the giant axon of Loligo. *The Journal of Physiology*, 116(4):449–472.

   In this paper, the membrane current is separated into Na^+ and K^+ components by manipulating the sodium content of the extracellular medium. Currents are recorded in voltage-clamp with an activation protocol (from rest to depolarized value).

3. Hodgkin, A. L. and Huxley, A. F. (1952). The components of membrane conductance in the giant axon of Loligo. *The Journal of Physiology*, 116(4):473–496.

   A deactivation protocol (voltage-clamp from depolarized value to rest) is used to demonstrate the linearity of instantaneous current-voltage relationships, meaning that conductances reflect permeabilities.

4. Hodgkin, A. L. and Huxley, A. F. (1952). The dual effect of membrane potential on sodium conductance in the giant axon of Loligo. *The Journal of Physiology*, 116(4):497–506.

   The inactivation of the Na^+ current is investigated using two-pulse voltage-clamp protocols.

5. Hodgkin, A. and Huxley, A. (1952). A quantitative description of membrane current and its application to conduction and excitation in nerve. *J Physiol (Lond)*, 117:500.

   The model is built from the previous papers and fitted to voltage-clamp measurements. It is then tested in a number of ways, in particular on various current-clamp and voltage-clamp protocols, and extended to a model of propagation (conduction velocity is predicted).

3.6 Summary and epistemological notes

3.6.1 Biophysics of action potentials

Work on the squid axon has shown that action potentials are produced by reversible changes in membrane permeability to specific ions. This mechanism appears to be at play in all excitable cells, not only squid axons. The explosive, regenerative, nature of the action potential is due to a positive feedback loop between membrane potential and membrane permeability to a specific ion species. A positive ion is more concentrated outside than inside the cell (Na^+ for the squid axon, Ca^{2+} for Paramecium), and membrane permeability to that ion increases with membrane

potential. As a result, stimulating the cell beyond a certain point produces an inward current, which depolarizes the membrane, leading to an even greater inward current, etc. In plants, a negative ion (Cl^-) is more concentrated inside than outside the cell and flows out at spike initiation, but the phenomenon is electrically equivalent. Thus the key biophysical ingredient of action potentials is voltage-dependent increase in specific permeability, or in modern terms voltage-dependent activation of ionic channels.

Repolarisation is due to a decrease in permeability to the same ion species and increase in K^+ permeability, both occurring slowly in comparison with than the rising phase of the action potential. These changes in permeability may also be voltage-dependent, as in the squid axon, or they may be triggered by the entry of the inward current, as in Paramecium.

3.6.2 Model making and model fitting

The Hodgkin-Huxley model recapitulates the above findings in a compact model, whose predictive power is remarkable. It is important to appreciate the epistemological nature of the model. First, it is primarily a model of the space-clamped squid axon, not a neuron model. It has been extended to a model of action potential propagation in the squid axon. Second, by construction, its relation to the natural system is through electrical variables (membrane potential, injected current) and ionic variables (ion fluxes and concentrations). The gating variables (m, n and h) have been introduced arbitrarily to fit the model to electrical experimental data but could be neither measured nor manipulated. In fact, they have no physical reality; later work has shown that the structure and dynamics of the channels are more complex than suggested by this model. As is explicitly stated in the original articles, the description of the model in terms of channel gates is only one possible interpretation of the equations. The models of the ionic currents are phenomenological; the key part of Hodgkin-Huxley theory is in fact the membrane equation:

$$C\frac{dV_m}{dt} + I_{Na} + I_K + I_L = I$$

This is the part of the model that has been subjected to experimental testing; the rest of the model is based on fitting measurements.

It is very instructive to understand the process of building the model, and the assumptions behind it. It is now common to start from assuming that neural excitability can be described by equations of the Hodgkin-Huxley type, and then to fit model parameters to experimental data. Parametric model fitting, however, is the trivial part of the process. Let us recapitulate the important assumptions behind the model:

1. Potential variations are only due to ionic and capacitive currents. This is the key assumption underlying the membrane equation and Hodgkin-Huxley theory in general. It is trivial when viewing the membrane as an electrical circuit, but this is only an analogy suggested by the theory. One could imagine for example that the distribution of ions around the membrane surface changes during excitation, or some more complex phenomenon involving the interaction of the membrane and associated structures with the intra- and extracellular medium, as proposed by Tasaki (2012). Other investigators have proposed that the action potential is primarily mechanical and electrical impulses are due to piezoelectric effects (Heimburg and Jackson, 2005).

2. Space can be ignored. The intracellular potential is assumed identical everywhere, and space-independent variables are used for gating variables and currents. In the axial direction, this is imposed by the experimental design, with a conducting wire inserted along the axon. For the propagating model, properties are considered uniform along the length of the axon.

3. The membrane current can be separated in specific ionic currents that do not directly interact with each other. It could have been, for example, that the passage of Na^+ and K^+ ions through the membrane is mediated by a shared mechanism, so that the two fluxes might not be independent.

4. Ionic currents can be expressed as the product of ion specific permeability with driving force $(V_m - E)$. This was shown with deactivation experiments. As we have previously discussed, this is not the generic case, as currents often follow GHK theory.

5. Permeability depends only on membrane potential. This is not the case in Paramecium, for example, where the inactivation of the Ca^{2+} current is mediated by intracellular Ca^{2+}. It could also be, for example, that mechanical changes in the membrane have an effect on permeability, through conformational changes in ionic channels (Anishkin et al., 2014).

6. Ion concentrations do not vary in either space or time. In principle, the entry of Na^+ and K^+ ions should change the concentrations of these ions, which in turn would change the amplitude of the ionic currents. This is neglected in the Hodgkin-Huxley model, on the basis that these changes should be very small in the large squid axon (see section **??**). From the assumption of uniformity of the squid axon membrane, it is also assumed that ionic concentrations are spatially constant. If this assumption were not valid, then one should consider axial diffusion currents in addition to the electrical term present in the cable equation.

This set of non-trivial assumptions forms the basis of the model; more specifically, of the first equation of the model (the membrane equation). The rest of the model (the three other equations) is an empirical quantitative description of the ionic currents, under the assumptions of the model. These are not expected to be universal. The model fitting component is necessary to make quantitative predictions. But it is important to realize that when these predictions are compared to experimental data, what is being tested is not so much the model itself as the theory behind it (mainly the ionic basis of the action potential). For example, the model can make a quantitative prediction of Na^+ influx during the action potential, which can be verified with radioactive tracers. This is a remarkable prediction as it only follows from the fitted model of the Na^+ current under the assumption that the change in membrane potential is mainly due to ionic currents.

Bibliography

Anishkin, A., Loukin, S. H., Teng, J., and Kung, C. (2014). Feeling the hidden mechanical forces in lipid bilayer is an original sense. *Proceedings of the National Academy of Sciences*, 111(22):7898–7905.

Armstrong, C. M. (2007). Life among the axons. *Annual Review of Physiology*, 69:1–18.

Armstrong, C. M. and Bezanilla, F. (1977). Inactivation of the sodium channel. II. Gating current experiments. *The Journal of General Physiology*, 70(5):567–590.

Astrm, K. J. and Murray, R. M. (2008). *Feedback Systems: An Introduction for Scientists and Engineers*. Princeton University Press, Princeton.

Attwell, D. and Laughlin, S. B. (2001). An Energy Budget for Signaling in the Grey Matter of the Brain. *Journal of Cerebral Blood Flow & Metabolism*, 21:1133–1145.

Baker, P. F., Hodgkin, A. L., and Ridgway, E. B. (1971). Depolarization and calcium entry in squid giant axons. *The Journal of Physiology*, 218(3):709–755.

Bal, T. and Destexhe, A., editors (2009). *Dynamic-Clamp*. Springer US, New York, NY.

Baranauskas, G., David, Y., and Fleidervish, I. A. (2013). Spatial mismatch between the Na+ flux and spike initiation in axon initial segment. *Proceedings of the National Academy of Sciences*, 110(10):4051–4056.

Bezanilla, F. and Armstrong, C. (1977). Inactivation of the sodium channel. I. Sodium current experiments. *The Journal of General Physiology*, 70(5):549–566.

Boyle, P. J. and Conway, E. J. (1941). Potassium accumulation in muscle and associated changes. *The Journal of Physiology*, 100(1):1–63.

Brehm, P., Dunlap, K., and Eckert, R. (1978). Calcium-dependent repolarization in Paramecium. *The Journal of Physiology*, 274:639–654.

Brehm, P. and Eckert, R. (1978). Calcium entry leads to inactivation of calcium channel in Paramecium. *Science*, 202(4373):1203–1206.

Brehm, P., Eckert, R., and Tillotson, D. (1980). Calcium-mediated inactivation of calcium current in Paramecium. *The Journal of Physiology*, 306:193–203.

Brennecke, R. and Lindemann, B. (1974). Design of a fast voltage clamp for biological membranes, using discontinuous feedback. *Rev Sci Instrum*, 45(5):656–61. undefined May Design of a fast voltage clamp for biological membranes, using discontinuous feedback 4826158 0034-6748 Journal Article http://www.ncbi.nlm.nih.gov/entrez/query.fcgi?cmd=Retrieve&db=PubMed&dopt=Citation&list_uids=4826158.

Brette, R. (2015). What is the most realistic single-compartment model of spike initiation? *PLoS computational biology*, 11(4):e1004114.

Brette, R. and Destexhe, A. (2012). Intracellular recording. In *Handbook of neural activity measurement*. Cambridge University Press.

Brette, R., Piwkowska, Z., Monier, C., Rudolph-Lilith, M., Fournier, J., Levy, M., Frgnac, Y., Bal, T., and Destexhe, A. (2008). High-resolution intracellular recordings using a real-time computational model of the electrode. *Neuron*, 59(3):379–91.

Carter, B. C. and Bean, B. P. (2009). Sodium entry during action potentials of mammalian central neurons: incomplete inactivation and reduced metabolic efficiency in fast-spiking neurons. *Neuron*, 64(6):898–909.

Clay, J. R. (1991). A paradox concerning ion permeation of the delayed rectifier potassium ion channel in squid giant axons. *The Journal of Physiology*, 444:499–511.

Clay, J. R. (2005). Axonal excitability revisited. *Progress in Biophysics and Molecular Biology*, 88(1):59–90.

Cole, K. S. (1949). Dynamic electrical characteristics of the squid axon membrane. *Arch. Sci. Physiol*, 3(25):3–25.

Cole, K. S. and Curtis, H. J. (1938). Electric Impedance of Nitella During Activity. *The Journal of General Physiology*, 22(1):37–64.

Cole, K. S. and Curtis, H. J. (1939). ELECTRIC IMPEDANCE OF THE SQUID GIANT AXON DURING ACTIVITY. *The Journal of General Physiology*, 22(5):649–670.

Cole, K. S. and Moore, J. W. (1960). Potassium Ion Current in the Squid Giant Axon. *Biophysical Journal*, 1(1):1–14.

De Loof, A. (1986). The electrical dimension of cells: the cell as a miniature electrophoresis chamber. *International Review of Cytology*, 104:251–352.

Dodge, F. A. and Frankenhaeuser, B. (1959). Sodium currents in the myelinated nerve fibre of Xenopus laevis investigated with the voltage clamp technique. *The Journal of Physiology*, 148(1):188–200.

Eccles, J. C. (1957). The physiology of nerve cells.

Eckert, R. and Brehm, P. (1979). Ionic mechanisms of excitation in Paramecium. *Annual Review of Biophysics and Bioengineering*, 8:353–383.

Eckert, R. and Chad, J. E. (1984). Inactivation of Ca channels. *Progress in Biophysics and Molecular Biology*, 44(3):215–267.

Eckert, R. and Naitoh, Y. (1970). Passive electrical properties of Paramecium and problems of ciliary coordination. *The Journal of General Physiology*, 55(4):467–483.

El Hady, A. and Machta, B. B. (2015). Mechanical surface waves accompany action potential propagation. *Nature Communications*, 6:6697.

Emiliani, V., Cohen, A. E., Deisseroth, K., and Husser, M. (2015). All-Optical Interrogation of Neural Circuits. *The Journal of Neuroscience: The Official Journal of the Society for Neuroscience*, 35(41):13917–13926.

Faisal, A. A., White, J. A., and Laughlin, S. B. (2005). Ion-Channel Noise Places Limits on the Miniaturization of the Brains Wiring. *Current Biology*, 15(12):1143–1149.

Fleidervish, I. A., Lasser-Ross, N., Gutnick, M. J., and Ross, W. N. (2010). Na+ imaging reveals little difference in action potential-evoked Na+ influx between axon and soma. *Nat Neurosci*, 13(7):852–860.

Frankenhaeuser, B. (1960). Sodium permeability in toad nerve and in squid nerve. *The Journal of Physiology*, 152(1):159–166.

Gentet, L. J., Stuart, G. J., and Clements, J. D. (2000). Direct measurement of specific membrane capacitance in neurons. *Biophysical Journal*, 79(1):314–320.

Gentet, L. J. and Williams, S. R. (2007). Dopamine gates action potential backpropagation in midbrain dopaminergic neurons. *The Journal of Neuroscience: The Official Journal of the Society for Neuroscience*, 27(8):1892–1901.

Gilly, W. F. and Armstrong, C. M. (1984). Threshold channels–a novel type of sodium channel in squid giant axon. *Nature*, 309(5967):448–450.

Goldman, D. E. (1943). Potential, Impedance, and Rectification in Membranes. *The Journal of General Physiology*, 27(1):37–60.

Hagiwara, S., Naka, K.-i., and Chichibu, S. (1964). Membrane Properties of Barnacle Muscle Fiber. *Science*, 143(3613):1446–1448.

Heimburg, T. and Jackson, A. D. (2005). On soliton propagation in biomembranes and nerves. *Proceedings of the National Academy of Sciences of the United States of America*, 102(28):9790–9795.

Hennessey, T. M. and Kung, C. (1984). An anticalmodulin drug, W-7, inhibits the voltage-dependent calcium current in Paramecium caudatum. *Journal of Experimental Biology*, 110(1):169–181.

Herndon, R. M. (1963). The fine structure of the Purkinje cell. *The Journal of Cell Biology*, 18(1):167–180.

Hill, B. C., Schubert, E. D., Nokes, M. A., and Michelson, R. P. (1977). Laser interferometer measurement of changes in crayfish axon diameter concurrent with action potential. *Science*, 196(4288):426–428.

Hille, B. (2001). *Ion Channels of Excitable Membranes*. Sinauer Associates. undefined 3rd Edition Ion Channels of Excitable Membranes.

Hodgkin, A. (1975). The optimum density of sodium channels in an unmyelinated nerve. *Philosophical Transactions of the Royal Society of London. Series B, Biological Sciences*, 270(908):297–300.

Hodgkin, A. and Huxley, A. (1939). Action Potentials Recorded from Inside a Nerve Fibre. *Nature*, 144(3651):710.

Hodgkin, A. and Huxley, A. (1952a). A quantitative description of membrane current and its application to conduction and excitation in nerve. *J Physiol (Lond)*, 117:500.

Hodgkin, A. L. (1951). The Ionic Basis of Electrical Activity in Nerve and Muscle. *Biological Reviews*, 26(4):339–409.

Hodgkin, A. L. (1964). *The conduction of the nervous impulse*. C. C. Thomas.

Hodgkin, A. L. and Huxley, A. F. (1952b). The components of membrane conductance in the giant axon of Loligo. *The Journal of Physiology*, 116(4):473–496.

Hodgkin, A. L. and Huxley, A. F. (1952c). Currents carried by sodium and potassium ions through the membrane of the giant axon of Loligo. *The Journal of Physiology*, 116(4):449–472.

Hodgkin, A. L. and Huxley, A. F. (1952d). The dual effect of membrane potential on sodium conductance in the giant axon of Loligo. *The Journal of Physiology*, 116(4):497–506.

Hodgkin, A. L., Huxley, A. F., and Katz, B. (1952). Measurement of current-voltage relations in the membrane of the giant axon of Loligo. *The Journal of Physiology*, 116(4):424–448.

Hodgkin, A. L. and Katz, B. (1949). The effect of sodium ions on the electrical activity of the giant axon of the squid. *The Journal of Physiology*, 108(1):37–77.

Hook, C. and Hildebrand, E. (1979). Excitation of paramecium. *Journal of Mathematical Biology*, 8(2):197–214.

Hoppensteadt, F. C. and Peskin, C. (2004). *Modeling and Simulation in Medicine and the Life Sciences*. Springer, New York, 2nd edition edition.

Hossain, W. A., Antic, S. D., Yang, Y., Rasband, M. N., and Morest, D. K. (2005). Where is the spike generator of the cochlear nerve? Voltage-gated sodium channels in the mouse cochlea. *The Journal of Neuroscience: The Official Journal of the Society for Neuroscience*, 25(29):6857–68.

Howarth, C., Gleeson, P., and Attwell, D. (2012). Updated Energy Budgets for Neural Computation in the Neocortex and Cerebellum. *Journal of Cerebral Blood Flow & Metabolism*, 32(7):1222–1232.

Husser, M., Stuart, G., Racca, C., and Sakmann, B. (1995). Axonal initiation and active dendritic propagation of action potentials in substantia nigra neurons. *Neuron*, 15(3):637–647.

Jacobson, K., Sheets, E. D., and Simson, R. (1995). Revisiting the fluid mosaic model of membranes. *Science (New York, N.Y.)*, 268(5216):1441–1442.

Kole, M. H. P., Ilschner, S. U., Kampa, B. M., Williams, S. R., Ruben, P. C., and Stuart, G. J. (2008). Action potential generation requires a high sodium channel density in the axon initial segment. *Nat Neurosci*, 11(2):178–186.

Kosaka, T. (1980). The axon initial segment as a synaptic site: Ultrastructure and synaptology of the initial segment of the pyramidal cell in the rat hippocampus (CA3 region). *Journal of Neurocytology*, 9(6):861–882.

Kramer, E. M. and Myers, D. R. (2013). Osmosis is not driven by water dilution. *Trends in Plant Science*, 18(4):195–197.

Kung, C. and Eckert, R. (1972). Genetic Modification of Electric Properties in an Excitable Membrane. *Proceedings of the National Academy of Sciences*, 69(1):93–97.

Kushmerick, M. J. and Podolsky, R. J. (1969). Ionic Mobility in Muscle Cells. *Science*, 166(3910):1297–1298.

Leterrier, C., Potier, J., Caillol, G., Debarnot, C., RuedaBoroni, F., and Dargent, B. (2015). Nanoscale Architecture of the Axon Initial Segment Reveals an Organized and Robust Scaffold. *Cell Reports*, 13(12):2781–2793.

Levin, M. (2014). Molecular bioelectricity: how endogenous voltage potentials control cell behavior and instruct pattern regulation in vivo. *Molecular Biology of the Cell*, 25(24):3835–3850.

Ling, G. and Gerard, R. W. (1949). The normal membrane potential of frog sartorius fibers. *Journal of Cellular Physiology*, 34(3):383–96.

Machemer, H. (1998). Electrophysiology. In Grtz, P. D. H.-D., editor, *Paramecium*, pages 185–215. Springer Berlin Heidelberg. DOI: 10.1007/978-3-642-73086-3_13.

Machemer, H. and Ogura, A. (1979). Ionic conductances of membranes in ciliated and deciliated Paramecium. *The Journal of Physiology*, 296:49–60.

Marmont, G. (1949). Studies on the axon membrane; a new method. *J Cell Physiol*, 34(3):351–82.

McLaughlin, S. (1977). Electrostatic Potentials at Membrane-Solution Interfaces. In Kleinzeller, F. B. a. A., editor, *Current Topics in Membranes and Transport*, volume 9, pages 71–144. Academic Press.

Molleman, A. (2002). *Patch Clamping: An Introductory Guide to Patch Clamp Electrophysiology*. Wiley-Blackwell, New York.

Morris, C. and Lecar, H. (1981). Voltage oscillations in the barnacle giant muscle fiber. *Biophysical Journal*, 35(1):193–213.

Naitoh, Y. and Eckert, R. (1968). Electrical properties of Paramecium caudatum: all-or-none electrogenesis. *Zeitschrift fr vergleichende Physiologie*, 61(4):453–472.

Naitoh, Y. and Eckert, R. (1973). Sensory Mechanisms in Paramecium. *Journal of Experimental Biology*, 59(1):53–65.

Naitoh, Y., Eckert, R., and Friedman, K. (1972). A Regenerative Calcium Response in Paramecium. *Journal of Experimental Biology*, 56(3):667–681.

Naitoh, Y. and Kaneko, H. (1972). Reactivated Triton-Extracted Models of Paramecium: Modification of Ciliary Movement by Calcium Ions. *Science*, 176(4034):523–524.

Nakada, C., Ritchie, K., Oba, Y., Nakamura, M., Hotta, Y., Iino, R., Kasai, R. S., Yamaguchi, K., Fujiwara, T., and Kusumi, A. (2003). Accumulation of anchored proteins forms membrane diffusion barriers during neuronal polarization. *Nature Cell Biology*, 5(7):626–632.

Narahashi, T., Moore, J. W., and Scott, W. R. (1964). Tetrodotoxin Blockage of Sodium Conductance Increase in Lobster Giant Axons. *The Journal of General Physiology*, 47(5):965–974.

Neher, E. and Sakmann, B. (1976). Single-channel currents recorded from membrane of denervated frog muscle fibres. *Nature*, 260(5554):799–802.

Oertel, D., Schein, S. J., and Kung, C. (1977). Separation of membrane currents using a Paramecium mutant. *Nature*, 268(5616):120–124.

Ogura, A. and Takahashi, K. (1976). Artificial deciliation causes loss of calcium-dependent responses in Paramecium. *Nature*, 264(5582):170–172.

Overton, E. (1902). Beitrge zur allgemeinen Muskel- und Nervenphysiologie. *Archiv fr die gesamte Physiologie des Menschen und der Tiere*, 92(3-5):115–280.

Patlak, J. (1991). Molecular kinetics of voltage-dependent Na+ channels. *Physiological Reviews*, 71(4):1047–1080.

Perge, J. A., Niven, J. E., Mugnaini, E., Balasubramanian, V., and Sterling, P. (2012). Why Do Axons Differ in Caliber? *The Journal of Neuroscience*, 32(2):626–638.

Peterson, B. Z., DeMaria, C. D., and Yue, D. T. (1999). Calmodulin Is the Ca2+ Sensor for Ca2+-Dependent Inactivation of L-Type Calcium Channels. *Neuron*, 22(3):549–558.

Phillips, R., Kondev, J., and Theriot, J. (2008). *Physical Biology of the Cell*. Garland Science, New York, 1 edition edition.

Purves, R. D. (1981). *Microelectrode methods for intracellular recording and ionophoresis*. Academic Press New York.

Ramon-y Cajal, S. (1899). *Texture of the Nervous System of Man and the Vertebrates*.

Rosen, R. (1985). *Anticipatory Systems: Philosophical, Mathematical and Methodological Foundations*. Pergamon Pr, Oxford u.a., 1st edition edition.

Saimi, Y. and Kung, C. (1987). Behavioral genetics of Paramecium. *Annual Review of Genetics*, 21:47–65.

Saimi, Y. and Kung, C. (1994). Ion channel regulation by calmodulin binding. *FEBS Letters*, 350(2):155–158.

Satow, Y. (1978). Internal calcium concentration and potassium permeability in Paramecium. *Journal of Neurobiology*, 9(1):81–91.

Satow, Y. and Kung, C. (1976). A TEA+-insensitive mutant with increased potassium conductance in Paramecium aurelia. *Journal of Experimental Biology*, 65(1):51–63.

Satow, Y. and Kung, C. (1980). Ca-Induced K+-Outward Current in Paramecium Tetraurelia. *Journal of Experimental Biology*, 88(1):293–304.

Sigworth, F. J. and Neher, E. (1980). Single Na channel currents observed in cultured rat muscle cells. *Nature*, 287(2):447.

Singer, S. J. and Nicolson, G. L. (1972). The Fluid Mosaic Model of the Structure of Cell Membranes. *Science*, 175(4023):720–731.

Stuart, G. J. and Sakmann, B. (1994). Active propagation of somatic action potentials into neocortical pyramidal cell dendrites. *Nature*, 367(6458):69–72.

Tasaki, I. (2012). *Physiology and Electrochemistry of Nerve Fibers*. Elsevier.

Tasaki, I., Nakaye, T., and Byrne, P. M. (1985). Rapid swelling of neurons during synaptic transmission in the bullfrog sympathetic ganglion. *Brain Research*, 331(2):363–365.

Thomas, R. C. (2009). The plasma membrane calcium ATPase (PMCA) of neurones is electroneutral and exchanges 2 H+ for each Ca2+ or Ba2+ ion extruded. *The Journal of Physiology*, 587(2):315–327.

Thome, C., Kelly, T., Yanez, A., Schultz, C., Engelhardt, M., Cambridge, S., Both, M., Draguhn, A., Beck, H., and Egorov, A. (2014). Axon-Carrying Dendrites Convey Privileged Synaptic Input in Hippocampal Neurons. *Neuron*, 83(6):1418–1430.

Tuckwell, H. (1988). *Introduction to theoretical neurobiology, vol 1: linear cable theory and dendritic structure*. Cambridge University Press, Cambridge. undefined Introduction to theoretical neurobiology, vol 1: linear cable theory and dendritic structure 3 NOT IN FILE.

Vandenberg, C. A. and Bezanilla, F. (1991a). Single-channel, macroscopic, and gating currents from sodium channels in the squid giant axon. *Biophysical Journal*, 60(6):1499–1510.

Vandenberg, C. A. and Bezanilla, F. (1991b). A sodium channel gating model based on single channel, macroscopic ionic, and gating currents in the squid giant axon. *Biophysical Journal*, 60(6):1511–1533.

Verkman, A. S. (2002). Solute and macromolecule diffusion in cellular aqueous compartments. *Trends in Biochemical Sciences*, 27(1):27–33.

Xu, K., Zhong, G., and Zhuang, X. (2013). Actin, Spectrin, and Associated Proteins Form a Periodic Cytoskeletal Structure in Axons. *Science*, 339(6118):452–456.

Young, J. Z. (1936). The Structure of Nerve Fibres in Cephalopods and Crustacea. *Proceedings of the Royal Society of London B: Biological Sciences*, 121(823):319–337.

List of Figures

Index